Bernhard Burtscher, BSc

Inkjet printed organic photodiode on an ultrathin, commercial, conformal and transferrable polymer substrate

MASTER'S THESIS

to achieve the university degree of

Diplom-Ingenieur

Master's degree programme: Technical Physics

submitted to

Graz University of Technology

Supervisor

Dr.Dott. Francesco Greco

Co Supervisor
Ao.Univ.-Prof.i.R. Dipl.-Ing. Dr.techn. tit.Univ.-Prof. Günther Leising

Institute of Solid State Physics

Graz, April 2019

AFFIDAVIT

I declare that I have authored this thesis independently, that I have not used other than the declared sources/resources, and that I have explicitly indicated all material which has been quoted either literally or by content from the sources used. The text document uploaded to TUGRAZonline is identical to the present master‘s thesis.

Date

Signature

Acknowledgement

Thank you ...

...especially to my supervisor Dr. Francesco Greco for his knowledge and great support, as well as helping me improve on a daily basis.

...to Prof. Leising for his expertise and input, whenever needed.

...to the people of the Institute of Solid State Physics for the warm welcome and the help during laboratory work.

...to my friends for memorable times on and off campus.

...to my family for always supporting me and lending a hand whenever and however they could.

Abstract

Personal health monitoring in the form of wearable and epidermal electronics has grown a lot of popularity. The use of novel materials and manufacturing processes are enabling a new generation of ultrathin, transferrable and imperceptible electronic devices for multiple applications. In order to enhance their application more devices (like organic photodiodes) on substrates that fulfil these requirements are investigated. First and foremost was the goal of this thesis to fabricate a transferrable organic photodiode (OPD) preferably through inkjet printing that could also be used for conformable and wearable electronics. Therefore, suitable easy to transfer, commercial polymer substrates were considered in the form of decal transfer tattoo-papers or a medical adhesive. These have the advantage of being flexible, low-cost and conformable, even to the point of being imperceptible. Target surfaces for final application include artificial (flat and smooth e.g. glass or even complex and rough, e.g. concrete, paper, plastic etc.) as well as natural ones (e.g. human skin).

To achieve this goal available substrates and materials were investigated. Especially the polymer substrate was crucial since not only the transferability was important for fabrication and/or application purposes but also their thickness, surface topography, surface wettability and optical properties.
The fabrication of a transferrable OPD started with using well-known materials with less emphasis on the fabrication process. Next steps included changing the materials to achieve a bulk heterojunction from a water-based, printable solution. Therefore, water-soluble polythiophene and fullerene derivatives were used and the printed film analysed regarding its thickness and absorbance.
Each layer composing an OPD was studied in detail individually and specific materials and fabrication solutions were chosen. For the transparent electrode the conducting polymer PEDOT:PSS[1] was chosen as it already has widely been used in OPDs and solar cells. Furthermore, it is inkjet printable, has good conductivity and shows high transparency.
Changing the other electrode from evaporated aluminium to non-vacuum-based alternatives for the second electrode was investigated. Moreover, two transparent electrodes (namely, printed PEDOT:PSS and AgNw[2] with printed AZO[3]), enabling its use from both sides and thus enhancing its application potential, were explored.
In the end possible OPDs were characterised through I/V-characteristic curve measurements to verify their proper functionality, even after transfer.

[1] Poly(3,4-ethylenedioxythiophene) polystyrene sulfonate
[2] silver nanowires
[3] aluminium doped zinc oxid

Zusammenfassung

Die persönliche Gesundheitsüberwachung in Form von tragbarer und epidermaler Elektronik hat in den letzten Jahren stark an Bedeutung gewonnen. Der Einsatz neuartiger Materialien und Herstellungsverfahren ermöglicht eine neue Generation ultradünner, übertragbarer, nicht spürbarer elektronischer Geräte für vielfältige Anwendungen. Um ihre Anwendung zu verbessern, werden weitere Geräte (wie organische Photodioden) auf Untergründen untersucht, die diese Anforderungen erfüllen.
In erster Linie war das Ziel dieser Arbeit, eine übertragbare organische Photodiode (OPD) herzustellen, vorzugsweise durch Inkjet-Druck, die auch für konforme und tragbare Elektronik verwendet werden könnte. Daher wurden geeignete, leicht zu übertragende, handelsübliche Polymersubstrate in Form von temporären Tattoo-Transferpapieren oder medizinischen Pflastern in Betracht gezogen. Diese haben den Vorteil flexibel, kostengünstig und konform zu sein, soweit dass sie nicht spürbar sind. Zieloberflächen für die Endanwendung sind sowohl künstliche (ebene und glatte z.B. Glas oder auch komplexe und raue, z.B. Beton, Papier, Kunststoff usw.) als auch natürliche (z.B. menschliche Haut).
Um dieses Ziel zu erreichen, mussten verwendbare Substrate und Materialien untersucht werden. Insbesondere das Polymersubstrat war entscheidend, da nicht nur die Übertragbarkeit wichtig ist, sondern auch deren Dicke, Oberflächentopographie, Oberflächenbenetzbarkeit und optische Eigenschaften.

Die Herstellung einer übertragbaren OPD begann mit der Verwendung bekannter Materialien, wobei der Schwerpunkt weniger auf dem Herstellungsprozess lag. Die nächsten Schritte waren die Änderung der Materialien, um einen Bulk-Heteroübergang aus einer wasserbasierten, druckbaren Lösung zu erreichen. Dazu wurden wasserlösliche Polythiophen- und Fullerenderivate verwendet und der gedruckte Film auf seine Dicke und Absorbanz analysiert.

Jede Schicht, aus der sich eine OPD zusammensetzt, wurde einzeln untersucht und es wurden spezifische Materialien und Fertigungslösungen ausgewählt. Für die transparente Elektrode wurde das leitende Polymer PEDOT:PSS gewählt, da es bereits in OPDs und Solarzellen weit verbreitet ist. Darüber hinaus kann es gedruckt werden, hat eine gute Leitfähigkeit und zeigt eine hohe Transparenz.
Die andere Elektrode wurde zunächst aus Aluminium aufgedampft. Danach wurden auch nicht-vakuumbasierte Alternativen für die zweite Elektrode berücksichtigt. Die OPD wurde dann mit zwei transparenten Elektroden (nämlich PEDOT:PSS und Ag Nw mit gedrucktem AZO) hergestellt, die ihre Verwendung von beiden Seiten ermöglichen und somit ihr Anwendungspotenzial erhöhen.
Am Ende wurden die möglichen OPDs durch I/V-Kennlinienmessungen charakterisiert, um ihre korrekte Funktionalität auch nach der Übertragung zu überprüfen.

Contents

List of Figures

List of Tables

Acronyms

AFM	atomic force microscopy
Ag Nw	silver nanowires
AZO	aluminium doped zinc oxid
AZO-electrode	combination of AZO and Ag Nw to an electrode
CA	Cellulose Acetate
CAM	contact angle measurement
CIJ	continuous inkjet
DoD	drop-on-demand
EBL	electron blocking layer
Fixomull	"Fixomull transparent": medical adhesive
HBL	hole blocking layer
ICBA	Indene-C_{60} bisadduct
MagicTouch	"Tattoo Transfer 2.1": tattoo-paper
OPD	organic photodiode
P3HT	Poly(3-hexylthiophene-2, 5-diyl)
P3P4T	Poly[3-(potassium-4-butanoate)thiophene-2, 5-diyl]
P3P5T	Poly[3-(potassium-5-pentanoate)thiophene-2, 5-diyl]
P3P6T	Poly[3-(potassium-6-hexanoate)thiophene-2, 5-diyl]
P3P7T	Poly[3-(potassium-7-heptanoate)thiophene-2, 5-diyl]
P3PXT	water-soluble polythiophene derivative
P3HT:ICBA (1:1 w/w)	solution of P3HT and ICBA in Toluene (1:1 w/w; 15 mg/ml P3HT/solvent)
P3P4T:PyC$_{60}$ (1:1 w/w)	ink solution of P3P4T and PyC$_{60}$ in 18 MΩ water (1:1 w/w; 10 mg/ml P3P4T/water)

PEDOT:PSS	Poly(3,4-ethylenedioxythiophene) polystyrene sulfonate
PJet 700	PEDOT:PSS ink
PTFE	Polytetrafluoroethylene
PyC$_{60}$	C_{60} Pyrrolidine tris-acid ethyl ester
SEM	scanning electron microscope
Silhouette	"Temporary Tattoo Paper": tattoo-paper
S1-series	Silhouette: one side washed
S2-series	Silhouette: both sides washed

Part I.

Introduction and fundamentals

1. Introduction

Wearable electronics [1] and lab-on-skin devices [2] gained a lot of interest over the last years. These epidermal sensors can obtain information from the skin about hydration, temperature, monitor electrophysiological signals [3] or oxygen blood level to name a few. While these offer great promise especially being imperceptible while worn, there still remain some problems like large-scale production possibilities, integration of power supply and data communication. [1, 2]
One way to address large-scale production could be printing techniques like inkjet, screen or gravure printing. Gravure and other roll-to-roll based techniques offer a high-volume and higher throughput compared to sheet-based ones, but are not as versatile. Inkjet printing as a non-contact fabrication technique also allows for low-cost and resource-friendly production. While the materials available at the moment are limited, ample possibilities exist and are further developed. Especially organic materials are of great interest as they concur with the demands for flexibility and sometimes even stretchability, while being usually solution processable, and thus, in principle, suitable for printing-based processing. [4] This makes them great candidates for manufacturing epidermal sensors and gained a lot of interest in this field.
For lab-on-skin devices or epidermal sensors the device needs to be transferred onto a target surface easily and adhere to it conformally, while ideally being flexible and stretchable. Beside these requirements, it should also be easy to handle and stable (mechanically and chemically). Thin polymer materials ($< 1\ \mu$m) show very good conformability [5] and are thus envisioned as optimal substrates for epidermal electronics. However, they are not easy to process and handle. An unconventional substrate, which has shown great promise is decal transfer temporary tattoo-paper, used as temporary tattoos for children. [1, 6]
In order to have a complete electronic system on board of such substrates, several electronic components are needed, as for example organic field-effect transistors. [5] Another problem is the embedding of a power supply; this has been addressed in different ways (fuel cell, batteries, power generation through energy harvesting, such as mechanical stress or with solar cells). Examples of the different powering strategies are nicely summarised by the recent reviews of Bandodkar *et al.* [1] and Liu *et al.* [2].
Organic photodiodes (OPDs) are another electrical component which are quite interesting as they could be used for receiving optical signals. This can be relevant in some bio-related application, such as e.g. to monitor blood oxygen level by pulse oximetry. Kim *et al.* [7] showed for example a battery-free, wireless pulse oximeter that is so small that it fits on a fingernail.
Some attempts to fabricate OPD[1]s on unconventional substrates have been reported,

[1] organic photodiode

as for example by Lamprecht *et al.* who used a newspaper as a substrate. [8]

Inspired by this, the question was what it takes to fabricate an OPD onto a commercial, transferrable substrate, such as decal transfer temporary tattoo-paper or a medical adhesive. Then it would not be necessary to fabricate the OPD directly onto the target surface, as it could be easily transferred to other surfaces. Easy transfer, flexibility and good conformability, up to the point of being imperceptible, are all properties desired by wearable electronics or lab-on-skin devices and therefore should be considered. Other questions regarded if it would be possible to have a flexible, low-cost, bio-compatible device that is inkjet printed or at least use other non-vacuum based techniques to allow for large-scale produced devices, that could also be skin-worn. To answer these, this thesis aims at producing a flexible, conformal, but most importantly transferrable OPD, preferably through inkjet printing, onto an ultrathin polymer substrate.
Several aspects need to be investigated to achieve this goal. First of all, what are the substrate possibilities and their properties. Materials and their solvents need to be investigated, regarding their compatibility with the substrate and toxicity. For this the idea is to use water-soluble materials (polythiophene and fullerene derivatives) for the active film. Another one is to have two transparent electrodes as these would allow the photodiode to work from both sides. Thus enhancing the application possibilities without having to change the layout. This may not be desired for all purposes like reflective pulse oximetry, where only reflected signals from the skin are essential.

2. Conformable and wearable electronics

As the name suggests conformable electronics is referring to unconventional flexible electronics systems which can adhere conformally to a target surface. Among these surfaces human skin is probably one of the most important, because of the interest in skin-worn devices for personal and health monitoring purposes. Therefore, conformal electronics is linked to wearable or epidermal electronics but not limited to. Particularly interesting for health monitoring, is the use of imperceptible substrate materials.

In Figure 2.1 an example is given how conformable electronics can look like. In this case a temporary tattoo was used. This has the advantage of being thin, flexible and even transparent. It shows how it adheres conformally to the surface, here a skin replica made of PDMS. This is possible because it is so thin. Temporary tattoos have been used as a substrate for electrodes to measure electrophysical properties like ECG, EMG or EEG. [3] Other examples for conformable electronics include organic field-effect transistors [5, 9], capacitors [10], organic amplifiers [11] and light-emitting electrochemical cells [12].

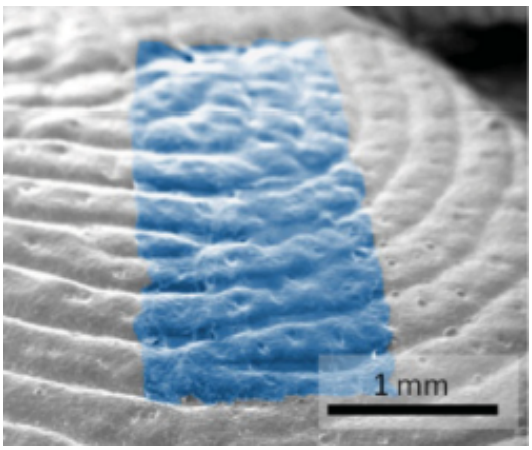

Figure 2.1.: Colourised SEM image of a PDMS-replica of human skin with a tattoo nanosheet [13]

More complex structures to even full devices have been developed. Yokota *et al.* showed for example the fabrication of polymer light-emitting diodes, organic photodetectors and their combination into a pulse oximeter. [14] Therefore, a 1 μm thick Parylene layer was used as a substrate material and the device laminated onto a finger. Other strategies for a pulse oximeter include for example a more rigid and thicker, but wireless design that is worn on a fingernail. [7]

Also tattoo-based electrochemical devices are investigated, making use of physiological relevant chemical constituents in biofluids. [1] Such electrochemical devices include pH sensors [15], sodium sensors [16] and epidermal biofuel cell [17] to state some.
Epidermal biofuel cells address another issue of such devices namely power supply. While some systems use NFC for powering [7] other strategies have been employed, like using piezoelectric [18] or triboelectric [19] effects.
Solar cells are another possibility. [20, 21, 22]

These are just a few examples of conformable and/or wearable electronics. They show its potential and the different direction one can think of. Especially a lot of the aforementioned sensor possibilities deal with health monitoring as it is one of the most looked at application for conformable electronics. The reason for this is that there the displacement through movements is negligible, which is a big improvement.

3. Organic photodiode (OPD)

Organic (carbon-based) electronics can be vacuum-deposited as small molecules or solution-processed, mostly in the form of conjugated polymers. Their appeal coming from the abundance of different synthetic small molecules and polymers and the resulting controllability of their properties.
The macroscopic properties of organic materials behave similar to their inorganic counterparts, but their microscopic behaviour differs fundamentally and therefore they have gained a lot of interest. While organic devices still are not performing as well as inorganic ones, interest in them is still high. This is primarily due to their low-cost, versatile production possibilities and resulting films that are extremely flexible, highly conformable and imperceptibly thin. This makes them very interesting for wearable and conformable devices and also for this thesis. These advantages yield application potential from OLEDs in displays [23] to completely new areas like electronic plants [24]. [25, 26, 27, 28]

Using organic materials in a photodiode allows for low-temperature process-ability (depending on the solvent) and using a wide variety of substrate materials as well as tweaking its properties for the application need, as for example bending or stretching. Therefore, organic materials were chosen for this thesis.

3.1. Basics

In a photodiode an electrical current is generated from light through the photoelectric effect. The basic structure of an OPD consists of a bottom electrode, a photoactive film and a top electrode as depicted in Figure 3.1. There it can also be seen that for this configuration the substrate and bottom electrode need to be transparent.

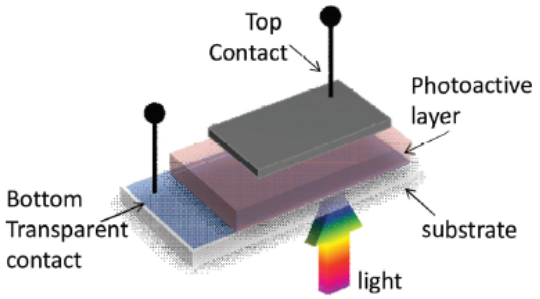

Figure 3.1.: Configuration of a vertical photodiode with light entering from the bottom. [29]

3. Organic photodiode (OPD)

In the photoactive region a photon can be absorbed and a bound electron-hole-pair (exciton or photogenerated exciton) is formed. This photogeneration has to compete against the following phenomena, here only their names will be mentioned without going into more detail (from [29]):

- radiative decay (ns time scale)
- exciton diffusion
- exciton quenching

In the photoactive region, consisting of donor and acceptors, an exciton can decay into a charge transfer state after reaching a donor/acceptor interface. There the electron is in the lowest unoccupied molecular orbital (LUMO) of the acceptor while the hole is in the highest occupied molecular orbital (HOMO) of the donor. In the charge transfer state the electron/hole-pair can dissociate more easy as their columbic attraction is less. While these exciton are formed in the donor they need to reach a donor/acceptor interface in their lifetime to be separated. Then they need to travel to the electrodes, where they can be collected. In Figure 3.2a the processes of photon absorption, charge separation and recombination at a donor/acceptor interface are illustrated. There also the energy levels of the HOMO and LUMO of the donor and acceptor are depicted. These are crucial for the functionality of the photodiode as they are responsible for photoinduced charge separation. While increasing the donor/acceptor LUMO offset can negatively impact the performance of a solar cell, it does not affect a photodetector negatively (as long as the Marcus inverted regime is not reached). This negative impact for solar cells is because there the power generation is the main focus, while for photodetectors the current signal is. The geometries for OPD and organic photovoltaics are similar, but have been optimised for different purposes.
The whole process from photon absorption to charge collection is primitively sketched in Figure 3.2b.

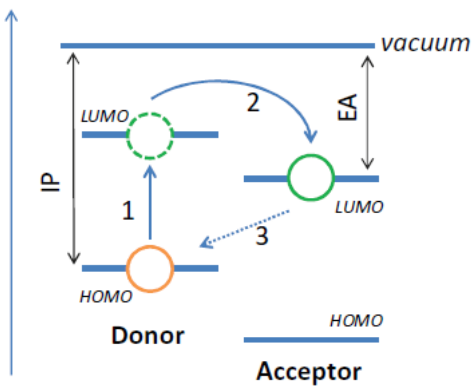

(a) Donor-Acceptor interface with assumed vacuum level alignment.
1... photon absorption;
2... charge separation;
3... recombination;
IP... ionization potential;
EA... electron affinity [29]

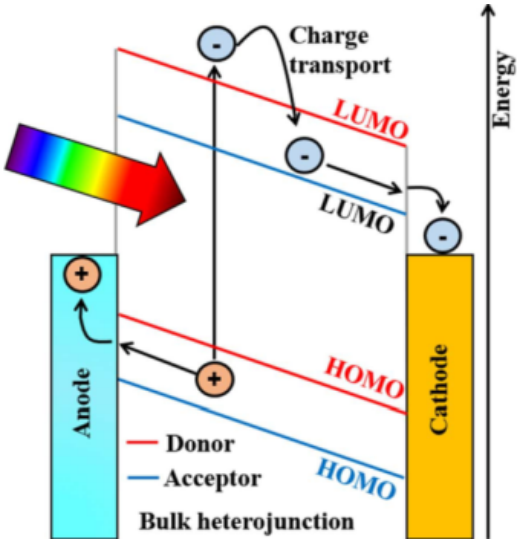

(b) Basic principle of charge generation in an OPD. [30]

Figure 3.2.: Schematic fundamentals OPD

3.2. Structures of the photoactive region

As the donor/acceptor interface is crucial for charge separation, possibilities to enhance it were looked at. At a simple planar heterojunction (Figure 3.3(a)), where the donor/acceptor interface is localised, only a very thin region at the interface will participate. Intermixing donor and acceptor in form of a bulk heterojunction (Figure 3.3(b)) will result in a bigger interface. There remain some problems with this geometry as not all donor or acceptor regions reach their designated electrode (dead-end transport paths) and also that at the electrodes both donor and acceptors are present, which can lead to recombination. Therefore, an ordered interpenetrated donor/acceptor system is thought of as an ideal structure (Figure 3.3(c)). [31] Here the focus is on bulk heterojunction OPD.

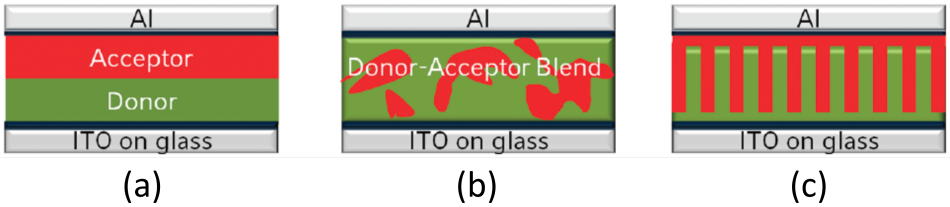

Figure 3.3.: Structure possibilties of photoactive film:
(a): bilayer planar heterojunction
(b): bulk heterojunction
(c): ordered interpenetrated donor/acceptor system [31]

3.3. Performance parameters

The performance of an OPD is affected by a lot of different factors like the carrier mobilities, geometry of the active region and energy level alignment of the whole device to name some examples.
Since quantifying these parameters is often hard, some figures of merits like the external quantum efficiency, responsivity, detectivity, signal-to-noise ratio, noise-equivalent power and response time or operation bandwith have been defined to compare different photodiodes. [32]
Since the main goal of this thesis is not to achieve the best performing device, but to provide a first proof of concept for the fabrication of a functioning OPD on an ultrathin, transferrable polymer substrate, these figures of merit will not be used. Instead an I/V-characteristic measurement will be performed to verify a photodiode behaviour. Such a characteristic curve is illustrated in Figure 3.4. The specific OPD reported in the example was made on a newspaper. [8]
The I/V-characteristic curve of Figure 3.4 shows the device behaviour in the dark and under illumination, as well as its typical behaviour in forward and reverse bias. Under illumination a photocurrent much higher than the dark current is observable in the reverse bias regime and slightly above zero.

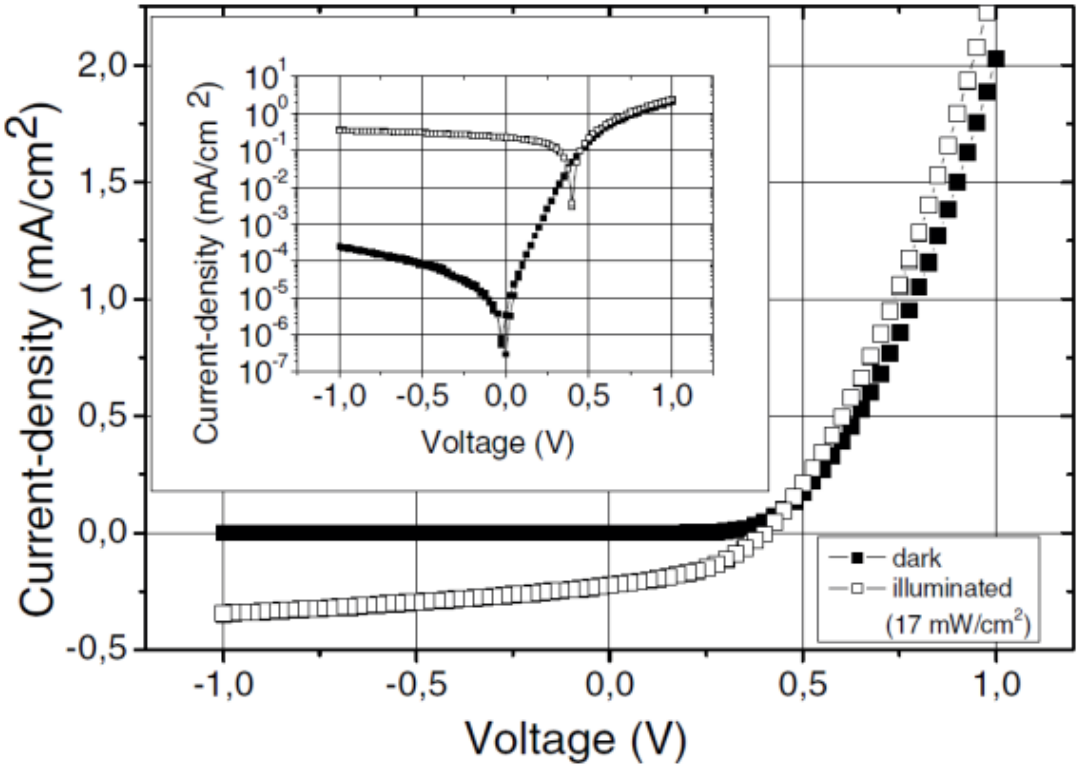

Figure 3.4.: Current density-voltage characteristic curve of an OPD. [8]

3.3.1. Reducing dark currents through adding blocking layers

Even in dark condition a current can be observable in the reverse bias regime and will negatively impact the performance by affecting the power consumption, photocurrent readout and the electronic noise. While many mechanisms can contribute to the electronic noise, the dominant part is assumed to origin from these dark currents. [33]
As an external voltage is applied, charge injection is expected, especially when the Fermi level of the metal is in the energy gap of the semiconductor. The preferred way to suppress the charge injection phenomena at the metal/semiconductor interface is by a high Schottky barrier. As bulk heterojunction configurations have a high probability that donors and acceptors are present at the metal/organic interface (Figure 3.5 (a)) the energy barrier is ill-defined and typically small. A way to improve this, is through a so-called vertically segregated bulk heterojunction (Figure 3.5 (b)).

Another possibility is given by including additional layers with the explicit purpose of blocking a specific charge carrier (holes or electrons), while not affecting the charge collection and/or the incident light (Figure 3.5 (c)).
These layouts with added layers can be problematic for photodiodes fabricated by solution-processing. Indeed, in this case the correct choice of compatible substrates, materials and orthogonal solvents, is very important, in order to not dissolve the underlying films or the substrate, while fabricating the multi-layered device structure.

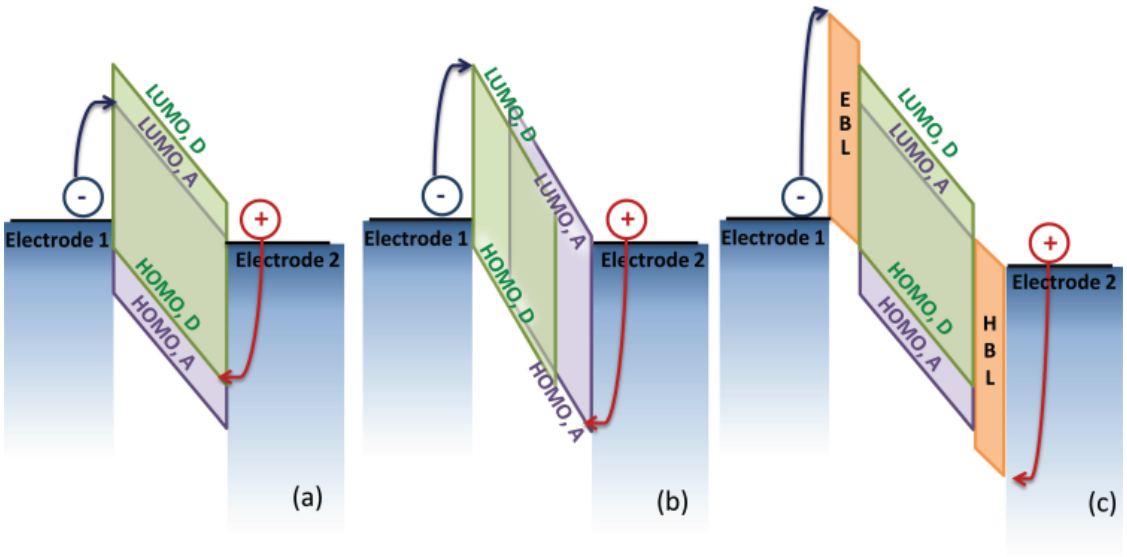

Figure 3.5.: Sketched charge injection phenomena at metal/active materials interface for
(a): generic donor/acceptor bulk heterojunction;
(b): vertically segregated bulk heterojunction;
(c): dedicated injection blocking layers.[29]
A. . . acceptor D. . . donor EBL. . . electron blocking layer HBL. . . hole blocking layer

This short overview about organic photodiodes is mostly based on the review "Organic Light Detectors" from Baeg *et al.* [29] with some information added from other sources. [32, 34, 35, 36]

3.4. Stability and degradation

Stability and degradation of OPDs and of organic solar cells still remain problematic. One can distinguish between intrinsic and extrinsic degradation, where intrinsic degradation arises mostly from thermal diffusion while extrinsic factors include temperature, light, oxygen, mechanical stress and humidity.
In order to improve device stability one can use either an encapsulation or engineer the interfaces carefully. Encapsulation helps protect the device from oxygen and water as well as enhancing mechanical stability. As glass plates can not be used for flexible systems to reduce known degradation factors as oxygen or water, other approaches were explored. These include bisphenol A-based epoxy resin [37], epoxy glue [38] or metal oxides with MgF_2 [39] for example.

As already mentioned in subsection 3.3.1 one can include additional layers to improve device performance, however processing of these additional layers can cause degradation of underlying layers and of the overall device. For example PEDOT:PSS is a hole transport layer commonly used in combination with ITO, but due to its acidic and hygroscopic behaviour corrodes ITO.
Similar is the situation for electron transport layers, where materials like LiF, Ca or ZnO are used but have high reactivity with oxygen, water, air and light. [30]

3.5. Recent works on OPD

Flexible OPD have been a highly regarded topic including new fabrication methods and incorporation into sensing devices. Here some examples of studies are presented, which have been published on the topic of OPD in the last two years, with the aim to provide a glimpse into recent advancements in the field.
One recent work reported of a full-colour pixel organic photodiode array with a single layer that is produced by blade coating and screen printing onto a flexible substrate, with a claimed RGB colour reconstruction of 98.5 %. To distinguish the colours three pixels detecting different colours are realised by spray coated filters. [40]
In another work OPDs were incorporated into an array for reflective oximeter to measure oxygen saturation and creating 2D oxygenation maps. [41]

Integrating OPDs into photoplethysmograph to estimate drowsiness was also investigated. [42]
Other groups improved device performance by using Cs_2CO_3-doped polyethyleneimine ethoxylated (d-PEIE) as electron transport layer, while obtaining good flexibility. There the normalised current variation remained above 90 % after bending it at a radius of 5 mm for 10 000 cycles, plus application possibility for optical luminescent oxygen sensors was shown. [43]

Also other directions were explored, to fabricate a high performance non-power-driven organic photodiode [44] or enhancing detection speed by addition of an insulating polymer [45], for example.

4. Deposition and characterisation methods

This chapter provides a basic introduction and background on the various deposition and measuring methods used in this thesis. The aim is to provide a short overview of the different techniques, enough to understand their basic principle.
In this thesis, in order to satisfy the requested demands for flexibility and conformability, organic materials were chosen for the top and active film. For their fabrication spin coating and inkjet printing were tested as deposition methods, with the ultimate goal to have a printed device. To fabricate a top electrode drop casting as well as thermal evaporation was used. Furthermore, to characterise the deposited films, methods such as profilometry, UV/VIS-spectroscopy or four-point-probe method were utilised.

4.1. Deposition methods

Several different deposition methods are used to fabricate thin films, and it is outside the scopes of this thesis to provide more than a basic introduction to them. Since thickness, homogeneity, low-cost and scalability are desired, inkjet printing would be a good choice. It also has the advantages of easy patterning and being resource friendly. Nevertheless, first deposition tests were made using spin coating, as inkjet printing with new inks needs some efforts for optimising inks formulation and printing parameters. Thus, their functionality was tested after spin coating. Another important step to achieve a homogeneous layer could be pre-deposition treatment of the surface. This could improve the adhesion between layers and surface wettability. As this would be the first step that has to be done, it will be discussed before spin coating and inkjet printing.

4.1.1. Pre-deposition treatment: plasma activation

Plasma, an ionized gas consisting of electrons, ions, radicals and photons, has neutral electrical charge. Here only its use for surface modification is of interest and therefore this introduction is limited to this application purpose and to artificially produced plasma. These are for example atmospheric pressure plasma jet, radio frequency discharge, microwave discharge and glow discharge.
Plasma can be defined by the gas used (air, oxygen, nitrogen, hydrogen, etc.), the pressure and the plasma mode. In industry atmospheric air plasma gained a lot of interest, because it does not need a vacuum and shows fast processing.
Plasma, through its reactivity, can modify plastic surfaces to make them harder, rougher,

more or less wettable, and favour adhesion. Choosing the right gas for a certain purpose can be crucial as for example oxygen-plasma increases while flourine-plasma decreases the surface energy of polymers. Increasing the surface energy will improve wettability of a fluid on a surface and therefore spreading. Simply put, if the same amount of liquid would cover a larger surface, it shows better wettability. One way to characterise this is to look at the contact angle, which a contact angle measurement (CAM) does. CAM is explained a little more in subsection 4.2.4.
Plasma can generate radicals from initiator molecules during polymerisation reaction or use radicals without any chemical reactions which were not observed before. Surface roughness also changes during plasma exposure and affect the wettability. However, it should be mentioned that the effect of surface "activation" (and thus on wettability of surfaces) is temporary. [46, 47, 48, 49]
For manufacturing purposes atmospheric plasma is of great interest and there have been different approaches utilised.

4.1.2. Spin coating

Spin coating has been studied and used for a rather long time as shown in the work of Emslie *et al.* [50] in 1958.
Following description is based on a review from Sahu *et al.* [51].

In spin coating centrifugal forces are used to produce a thin, homogeneous layer by depositing a solvent onto a rotating substrate. Therefore, the substrate is fixed on a spinner chuck by low vacuum before spinning.
The main steps in this process are deposition of fluid, spin-up, spin-off and evaporation. These steps are also illustrated in Figure 4.1.

- Deposition of fluid:
  Dispense can occur before starting the spin process or while rotating at low speed. For good control over the deposited volume especially when dispensing while rotating a micropipette can be used. Which deposition technique is used will be based on the fluid properties (primarily its viscosity) and its interaction with the substrate. Sometimes a surface treatment beforehand helps improving the coating parameters.
  To ensure the whole substrate is covered, an excessive amount of fluid is deposited and different techniques for dispensing can be used. These are more important when depositing while rotating, as in the not-rotating case covering of the substrate is easier controlled.
- Spin-up:
  In this stage through acceleration the excessive fluid on the substrate is forced off. This contributes to the formation of a homogeneous film as any thickness

differences will be smoothed out.

- Spin-off:
  During spin-off the substrate rotates at constant speed and the film becomes gradually thinner as more and more fluid is pushed to the edge where it can leave the substrate in droplets. Therefore, edge effects can occur.
- Evaporation:
  In this stage thinning of the film occurs because the solvent evaporates. The key difference in the spin-off and evaporation stage lies in the nature of how the thinning happens. While during spin-off fluid is flung off the substrate, only the solvent evaporates in the evaporation stage so that the solid part of the fluid can form a film. These two stages can also occur simultaneously.

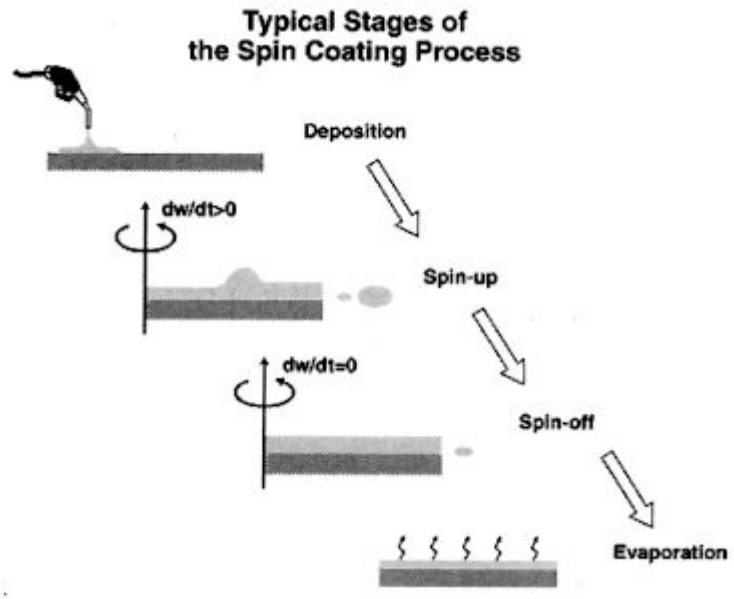

Figure 4.1.: Main steps of spin coating [51]

4.1.3. Inkjet printing

Generally, two main modes for operation are considered, namely continuous inkjet (CIJ) and drop-on-demand (DoD) printing. DoD is the main focus for this work with jetting of droplets induced by piezoelectric actuators. Even though the piezoelectric element can be further categorised, it is out of scope for this work. The interested reader is referred to the review of Cummins & Desmulliez [52] for further information. The working principle of a piezoelectric DoD-inkjet printer is schematically shown in Figure 4.2. Number of nozzles can vary largely from research to industrial printer. As in Figure 4.2 illustrated, the piezoelectric actuator can be controlled digitally by a

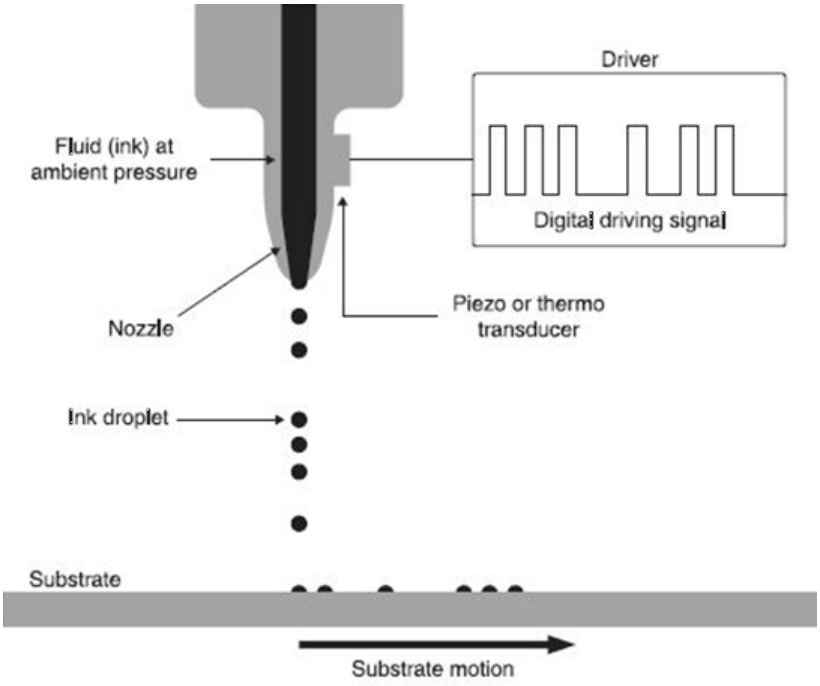

Figure 4.2.: DoD inkjet printing system [53]

computer program. This also allows for generating patterns by converting graphics into patterns of droplets.
Singh *et al.* [54] divided DoD-inkjet printing into five stages: drop ejection, drop flight, drop impact, drop spreading and drop solidification. Others often only distinguish three main parts: drop ejection and flight, drop impact and spreading, and drop solidification as for example Cummins & Desmulliez [52].

- Drop ejection and flight:
  An electric signal to the piezoelectric actuator reduces the volume of the ink chamber, resulting in a pressure rise. This also leads to an increase in kinetic energy due to the pressure wave and a droplet will be ejected if the surface tension is overcome.
  Drop shape is mostly influenced by the fluid properties, nozzle geometry and the signal applied to piezoelectric actuator, in print programs often referred to as waveforms. The shape can change during flight.
- Drop impact and spreading:
  The minimum feature size is determined in this stage and there are different indicators which classify if drop impact or spreading is dominant. Examples are Reynolds, Weber and Ohnesorge numbers. Mainly kinetic energy will be dissipated by impact and transformed into surface energy in the form of spreading.
- Drop solidification:
  Evaporation and polymerisation are some of the possible mechanism to occur

during phase change. Evaporation results in a volume change which can be very large and therefore significantly influence the final film properties. One drying phenomena is called "coffee staining" and defines the increased evaporation that happens at the edge and internal flow will result in a higher solid concentration. This can look like rings left behind by a coffee mug, hence the name.

This description of inkjet printing is based on the work of Cummins & Desmulliez [52], Prudenziati & Hormadaly [53] and Al-Halhouli *et al.* [4] unless otherwise stated.

4.1.4. Physical vapour deposition (PVD): thermal evaporation

PVD generally includes the techniques of evaporation, ion plating and sputtering and can produce films as thin as a few $\mathring{A}$. For this thesis thermal evaporation with a resistive heating was used.
Thermal evaporation is a vacuum-based technique, where through heating a material (mostly metal) will evaporate and due to the low pressure can adsorb and deposit on an in-line-of-sight surface. Through physical masking a desired pattern can be achieved. While thermal evaporation has advantages like high purity of films, excellent bonding to the surface, good control over film thickness and being able to deposit virtually any metal or alloy and even some organic materials, its costs and scalability are limiting it. [55]

4.2. Characterisation methods

Characterisation of the layers in this work include properties like thickness, surface wettability, optical transmittance as well as resistance measurements for semiconductors and conducting films.

4.2.1. Profilometry: thickness, roughness

Predominantly used to determine a step height, it is also possible to measure a sample's roughness. A stylus tip is placed in contact with the sample surface to be investigated and pressed against it with an adjustable and controlled load. Then the tip is dragged along a line and the change in height can be measured by linear variable differential transducer, optical lever or linear variable differential capacitor for example. [56]
For the height measurement a sharp edge is preferred (e.g. scratch) as well as a smooth underlying structure (e.g. Si-Wafer), so small heights can be detected and are not disturbed by the substrate roughness. To enhance the sensibility, external vibrations from the environment (e.g. air fluxes, vibrations of building and instruments), need to be minimised. This is typically obtained by isolating the measurement apparatus by placing it on top of an optical table and/or on top of a vibration dampening active

device. Moreover, a closed lid or cabinet is used to minimise air fluxes inside the measurement area.

4.2.2. Atomic force microscopy (AFM): roughness

AFM or scanning force microscope (SFM) scans across a surface area with a very sharp tip on a cantilever and because of this, through attractive and repulsive forces a topographic image is constructed. There are different ways the AFM can operate, for example, contact and tapping mode.
Piezocrystals are used to bring the sample in contact with the tip by moving one of them or both. The slight displacement of the cantilever can be observed by a reflected laser beam from the top side of the cantilever and measure via a photodetector. This kind of signal observation is called "optical lever" method. [57]
In this thesis it was used to determine the surface roughness.

4.2.3. UV/VIS-spectroscopy: absorbance, transmittance

Absorption of light in the UV and visible range by molecular species causes excitation of electrons from a full into an empty anti-bonding orbital. UV/VIS-spectroscopy is an important tool in optoelectronics to configure and customise the layer structure, so that the transparent electrode is really invisible in a certain range. A common system is a dual-beam spectrophotometer where the light is split up into two paths so the sample and a reference measurement can be taken simultaneously, as shown in Figure 4.3. This way the cuvette or reference glass substrate can be subtracted from the measurement and only the sample is observed.
Typically, either the absorbance or the transmittance is measured in such an experiment. The transmittance is defined as the ratio of transmitted to initial intensity. Absorbance is given by the product of thickness, the molar absorption coefficient and the molar concentration or through the Lambert-Beer law as:

$$A = -\log_{10}\frac{I_t}{I_i} = -\log_{10}T \tag{4.1}$$

A...	absorbance	I_t...	transmitted intensity
I_i...	initial intensity	T...	transmittance

For this thesis the transmittance will be used to investigate the transparent electrode and the absorbance to get the absorption spectrum of the active material. [58]

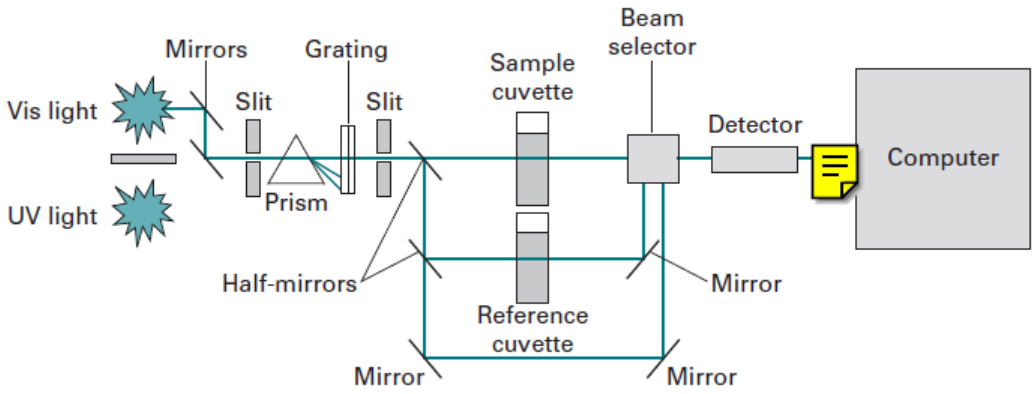

Figure 4.3.: Dual-beam spectrophotometer with a grating as monochromator [58].

4.2.4. Contact angle measurement (CAM): wettability

CAM is in close relationship to the Young–Dupré equation (Equation 4.2) and gives information about the interaction of liquid-solid, liquid-vapour and solid-vapour interface, or moreover, the wettability of a liquid on a surface. Therefore, not only the material is important but also its roughness, homogeneity and if it is free of impurities. Depending on the angle of the liquid-solid interface one can distinguish for example between hydrophilic and hydrophobic behaviour. [59]
Pending on the application purpose a certain performance is preferred and employing a surface treatment (e.g. plasma activation) may help to enhance the desired behaviour.

$$\gamma_{LV} \cos\theta = \gamma_{SV} - \gamma_{SL} \tag{4.2}$$

γ_{LV} ... liquid-vapour surface tension
γ_{SV} ... solid-vapour surface tension
θ ... contact angle
γ_{SL} ... solid-liquid surface tension

4.2.5. Four-point-probe method: sheet resistance

The four-point-probe measurement can be used to determine the sheet resistance of a material or, if the thickness of the thin film is known, to calculate its specific conductivity.
In Figure 4.4 the schematic structure can be seen, with four probes in linear assembly. These are in contact with a flat surface and a current passed through the outer electrodes, while the potential is measured across the inner electrodes (marked as 1 and 2).

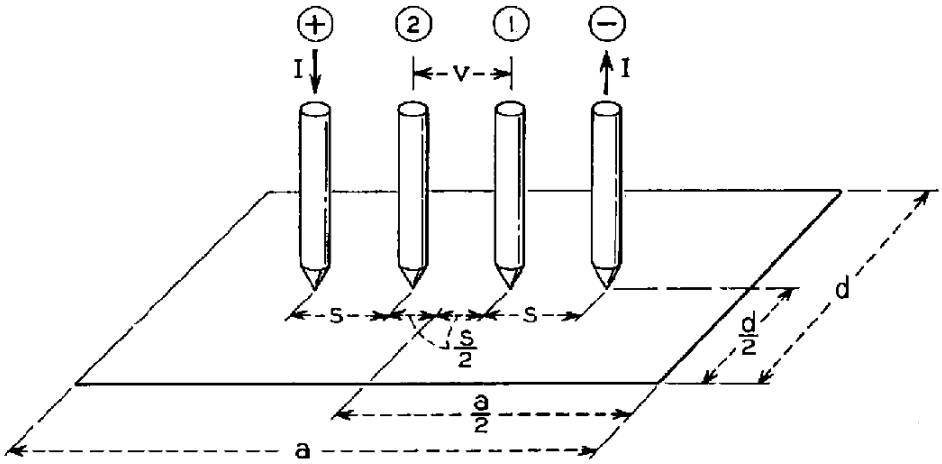

Figure 4.4.: Schematic illustration of a four-point-probe on a 2-dim., finite rectangular sample [60]. I... current, V... voltage, s... distance between probes, a, d... length and width of sample area

For sheet-like samples Equation 4.3 can be used to determine the sheet resistance.

$$\rho_s = \frac{V}{I} \frac{\pi}{ln(2)} \; C(a,s,d) \tag{4.3}$$

ρ_s... sheet resistivity

V...	voltage	I...	current
a...	length of sample area	d...	width of sample area
s...	spacing of probes	C(a,s,d)...	correction factor depending on a, s and d

For large sample areas the correction factor $C(a,s,d) \cong 1$, but careful some literature give the constant term $\pi/ln(2)$ into the correction factor. This equation is also only valid for sheet-like structures, for others a correction factor depending on the film thickness needs to be considered.
When the film thickness (t) is smaller than the half of the probe spacing (s)[$t < s/2$], there is a simple correlation between the measured sheet resistivity and the bulk resistivity [61], as given in Equation 4.4.

$$\rho = \rho_s \; t \tag{4.4}$$

ρ... bulk resistivity t... thickness

This description is based on the works of Smits [60] and Valdes [62].
In order to determine the resistivity/conductivity of fabricated electrodes this method will be employed.

Part II.

Materials and experimental setup

5. Materials

Here the used chemicals, substrates and additional materials are detailed, as well as a description of the ink preparation. Investigated substrate materials and all considered polythiophene and fullerene derivatives are specified in Table 5.1 and their chemical structures shown in Figure 5.1 and Figure 5.2.

Table 5.1.: List of considered substrates, polythiophene and fullerene derivatives

Abbreviation	Company	Product name	Description
MagicTouch	TheMagicTouch GmbH	Tattoo Transfer 2.1	decal transfer tattoo-paper
Silhouette	Silhouette America Inc.	Temporary Tattoo Paper	decal transfer tattoo-paper
Fixomull	BSN medical GmbH	Fixomull transparent	medical adhesive
P3HT	Rieke Metals Catalogue Nr.: 4002-E	Poly(3-hexylthiophene-2, 5-diyl)	polythiophene
ICBA	Aldrich 753955 – 250MG	Indene-C_{60} bisadduct	fullerene
P3P4T	Rieke Metals Catalogue Nr.: 4021	Poly[3-(potassium-4-butanoate)thiophene-2, 5-diyl]	polythiophene water-soluble
P3P5T	Rieke Metals Catalogue Nr.: 4022	Poly[3-(potassium-5-pentanoate)thiophene-2, 5-diyl]	polythiophene water-soluble
P3P6T	Rieke Metals Catalogue Nr.: 4024	Poly[3-(potassium-6-hexanoate)thiophene-2, 5-diyl]	polythiophene water-soluble
P3P7T	Rieke Metals Catalogue Nr.: 4026	Poly[3-(potassium-7-heptanoate)thiophene-2, 5-diyl]	polythiophene water-soluble
PyC_{60}	Aldrich 709093 – 250MG	C_{60} Pyrrolidine tris-acid ethyl ester	fullerene water-soluble

In Table 5.2 commercial inks and other materials like filter syringes, solvent and so on are listed.

Table 5.2.: Commercial inks and other materials

Abbreviation	Company	Product name	Description
PJet 700	Heraues	Clevious™ PJet 700	PEDOT:PSS ink
Ag Nw	Aldrich	778095 - 25ML	silver nanowires
AZO ink	Distributer: Aldrich Manufacturer: Genes'Ink	H-DZ01015	aluminium doped zinc oxid; nanoparticle ink
Filter CA	DIA-Nielsen GmbH & Co. KG	FCA300020	0.20 μm syringe filter Cellulose Acetate
Filter PTFE	DIA-Nielsen GmbH & Co. KG	FPT150020	0.20 μm syringe filter Polytetrafluoroethylene
Aluminium(Al)	umicore	0481534	evaporation material
Silver (Ag)	Aldrich	327050-10G	evaporation material
Toluene	Aldrich	34866 - 1L - M	organic solvent

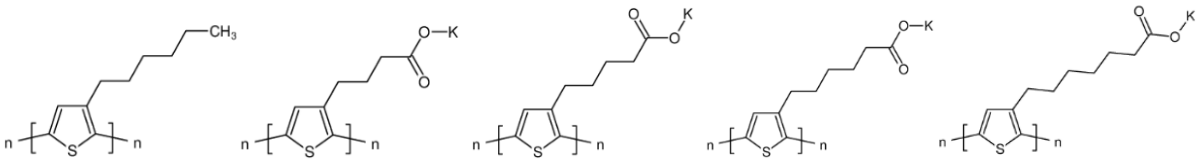

(a) P3HT [63] (b) P3P4T [64] water-soluble (c) P3P5T [65] water-soluble (d) P3P6T [66] water-soluble (e) P3P7T [67] water-soluble

Figure 5.1.: Chemical structure of polythiophene derivatives

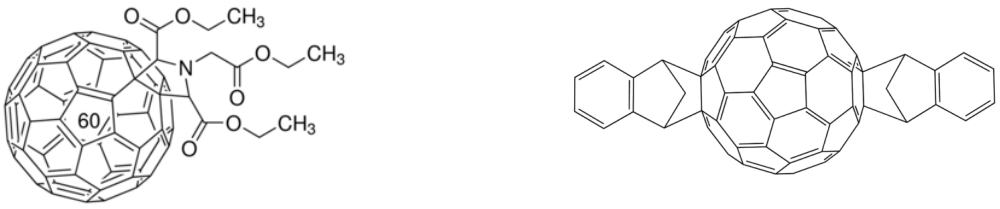

(a) Water-soluble fullerene: PyC_{60} [68] (b) ICBA [69]

Figure 5.2.: Fullerene derivatives: chemical structure

5.1. Substrate candidates

This work has been limited to consider three different materials as a transferrable substrate. Two of them are decal transfer tattoo-papers and the third is a medical adhesive. All of these three materials are commercially available.

The two decal transfer temporary tattoo-papers are "Tattoo Transfer 2.1" from TheMagicTouch GmbH and "Temporary Tattoo Paper" from Silhouette America Inc. These will be referred to as MagicTouch and Silhouette respectively. Both have a similar structure since both consist of a two sheet kit. The first sheet "Sheet A" consist of 3 or 4 layers. The bottom layer is silicone paper. On top of it a water-soluble sacrificial layer like Dextrin, starch or Polyvinyl alcohol (PVA) is placed. Because of this water-soluble layer the transfer is possible. The next layer is a material like Ethyl cellulose or Polyurethane + allyl resin. This is the whole structure for MagicTouch, while Silhouette has an additional topmost water-soluble layer.
The second sheet "Sheet B" is nearly identical for both. It is a layer of acrylic glue sandwiched between two release liners, which can be peeled off individually. The composition of the glue might be different but has no influence on this work. An illustration of their layouts can be seen in Figure 5.3.
Since Silhouette has an additional water-soluble layer it was also investigated when both of these were removed. Therefore, the Silhouette tattoo-paper without the bottom layers is considered as S1-series and when both sides were washed away and therefore all water solvable layers eliminated, is named S2-series. The schematic is illustrated in Figure 5.4.

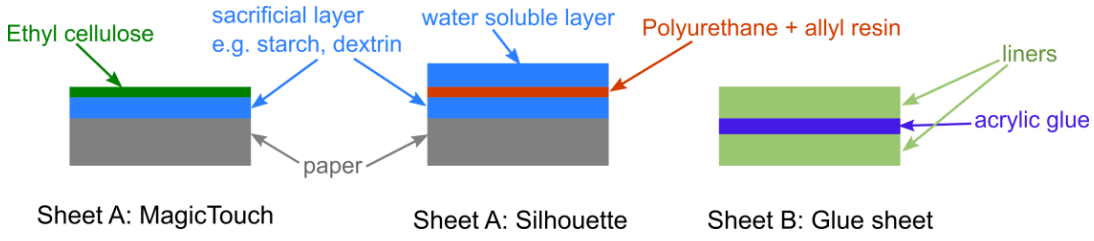

Figure 5.3.: Composition of decal transfer tattoo-papers MagicTouch and Silhouette

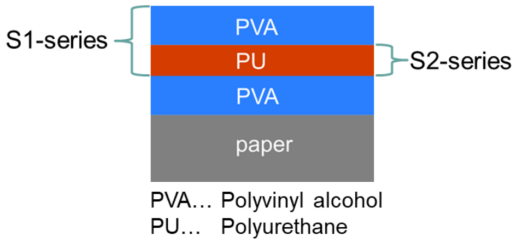

Figure 5.4.: Considered cases of Silhouette tattoo-paper

The transfer of both decal transfer tattoo-papers is the same although both can be attached with or without glue. In case of using glue, one protection layer of the glue sheet is removed and laminated onto the tattoo-paper. After peeling off the second liner of the glue sheet it can be attached to the target surface. Lastly the paper backside is wet with water to dissolve the sacrificial layer and then the paper is slided off.
Without using a glue, the tattoo-paper is positioned on the target surface so that the paper faces up. After applying water to the paper, thus removing the sacrificial layer and the paper can be slid off.

The medical adhesive is a product from BSN medical GmbH called "Fixomull transparent", here the abbreviation is Fixomull. One side of it is adhesive, which is covered with a paper-like protection layer. This liner can be peeled off to attach the adhesive side to the skin (or other surface). Afterwards the protective back layer is removed. In contrast to the tattoo-papers the releasable layer is thicker as it can be handled while free-standing.

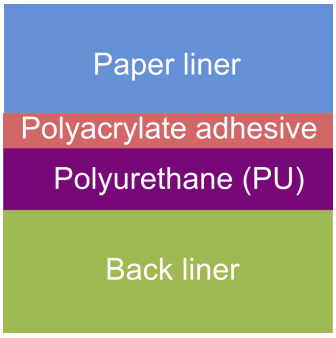

Figure 5.5.: Composition of medical adhesive Fixomull

5.2. Ink preparation

Here the focus is on how the inks were prepared or processed. The distributors of the materials are given in Table 5.1 and Table 5.2. Some of these were commercially available and just need some processing.

PJet 700 (PEDOT:PSS)

For the PEDOT:PSS film PJet 700 from Heraues was used after filtering it with a 0.20 μm CA[1] filter syringe and stored for some hours to get rid of any air bubbles. PJet 700 is an aqueous dispersion with a solid content of 0.6 - 1.2 % and it has a specified minimum conductivity of 650 S/cm. [70]

AZO ink

The AZO ink (H-DZ01015) was filtered with a 0.20 μm PTFE[2] filter and the cartridge stored wrapped in aluminium foil. Solvents for this ink are α-Terpineol and n-Butanol, while having a solid content of $\geq 1 - < 2.5$ %.

[1] Cellulose Acetate
[2] Polytetrafluoroethylene

Ag Nw

Ag Nw (778095 - 25ML) from Aldrich are suspended in 0.5 wt.% isopropyl alcohol. They have a diameter of 120 - 150 nm and a length of 20 - 50 μm.

P3HT and ICBA solution

P3HT and ICBA were dissolved in a ratio of 1:1 w/w in toluene with 15 mg/ml of P3HT/solvent. After stirring for about 24 h at 80 °C, temperature was reduced to 50 °C. Before use the solution was filtered with a 0.20 μm PTFE syringe filter. The solution was wrapped in aluminium foil to protect it from light.

Water-soluble polythiophene and fullerene derivative

A water-based solution (ink) for the active layer can be prepared by mixing a polythiophene (P3PXT[3]) and the fullerene (PyC_{60}) derivative with 18 MΩ water, heated to 80 °C, stirred until it was filtered with a 0.20 μm CA filter and filled into a cartridge. The stirring time may vary with the specific derivative but it exceeded 24 h in all cases. The temperature was reduced after 24 h to 50 °C and continuous stirring was applied as a precaution step as well as wrapping it in aluminium foil.
Only the polythiophene derivatives with the shortest (P3P4T) and longest (P3P7T) sidechain were looked at and their preparation varied slightly. For the ink solution P3P4T:PyC_{60} (1:1 w/w) P3P4T and PyC_{60} were mixed in a ratio of 1:1 w/w with 10 mg of P3P4T per ml of 18 MΩ water. The P3P7T:PyC_{60} (1:1 w/w) ink was prepared by mixing P3P7T and PyC_{60} (1:1 w/w) with 18 MΩ water in a ratio of 6.6 mg P3P7T per ml water.

18 MΩ water was gained from a water purification system from Sartorius AG (listed in Table 6.1). These inks should also be stored for some hours after filtering and before printing to get rid of air bubbles.

[3] water-soluble polythiophene derivative

6. Experimental setups and methods

6.1. Methodology

A summary over what was done and the reasoning behind ordering this thesis is given for better understanding.
Suitable polymer substrates were investigated regarding their thickness (profilometry), roughness (profilometry, AFM), wettability (CAM[1]) and transmittance (UV/VIS-spectrophotometry). During this set of preliminary measurements, it was obvious that some polymer substrates do not fulfil the desired properties, so they were discarded and not fully characterised.

After determining the best suitable substrate and defining the structure (inverse: first depositing transparent layer), the printing parameters for a commercial PEDOT:PSS-ink could be determined. In order to achieve a homogeneous film plasma activation of the substrate was needed.

For the bulk heterojunction polythiophene and fullerene derivatives were considered. Starting with better known materials (P3HT and ICBA) a solvent (compatible with substrate) was searched for spin coating. Toluene was found as a suitable solution.
As regards to the top electrode, some tests were made to investigate the use of a printable reactive silver-ink. Afterwards, based on unsatisfactory results, aluminium was evaporated to obtain a light response in the open-circuit potential. No characterisation of this layout was made at this point, as finding a printed active film and a vacuum-free fabricated bottom electrode were prioritised.
As constituents of the active film, various water-soluble polythiophene and fullerene derivatives were investigated. Four different polythiophenes with varying length of their side-chain could be chosen. Their water solubility arises from a potassium carboxylate salt side-chain. First tests were performed with the shortest side-chain polymer. After fabricating a prototype by spin coating (P3P4T:PyC_{60} (1:1 w/w)[2] on printed PEDOT:PSS) and an evaporated aluminium, its functionality was verified. Again this was viewed as a stepping stone and no I/V-characterisation was done. So next was finding printing parameters for this ink. In the end a serviceable printing process was found for this new ink. A sample was prepared with a printed active film and an evaporated aluminium layer on glass to observe a light response in the open-circuit potential.

[1] contact angle measurement
[2] ink solution of P3P4T and PyC_{60} in 18 MΩ water (1:1 w/w; 10 mg/ml P3P4T/water)

For the idea of a second semi-transparent electrode a commercial AZO ink was introduced, but due to its low conductivity, it was used in combination with Ag Nw (AZO-electrode[3]). Tests showed that the Ag Nw suspended in isopropyl alcohol destroy the underlying layers when deposited on top of them and that a spin coated film of Ag Nw was very bad conductive. To avoid damage to the other layers, the electrode was fabricated separately and combined with the rest through lamination. To achieve a low sheet resistance different deposition approaches were explored (spin coating, drop casting and drop casting onto a printed AZO layer). The best results could be achieved when printing an AZO layer and then depositing Ag Nw in two steps.

As it turned out the I/V-characteristic curve of the OPD with printed PEDOT:PSS/ P3P4T:PyC_{60} (1:1 w/w) and AZO-electrode were not as good as hoped. Therefore the device structures with PEDOT:PSS/P3HT:ICBA (1:1 w/w)[4] /Al and PEDOT:PSS/ P3P4T:PyC_{60} (1:1 w/w) /Al were also looked at. Some samples were then transferred onto a glass slide firstly to observe the effect of transfer and secondly not to measure through the back paper of the tattoo-paper.
Firstly the one with a printed PEDOT:PSS film, spin coated P3HT:ICBA (1:1 w/w) and evaporated aluminium is given as it was the first functioning OPD. Then one with printed PEDOT:PSS, printed P3P4T:PyC_{60} (1:1 w/w) and evaporated aluminium, which was prepared on glass is shown and lastly one is given with printed PEDOT:PSS, printed P3P4T:PyC_{60} (1:1 w/w) and AZO-electrode (Figure 6.1).

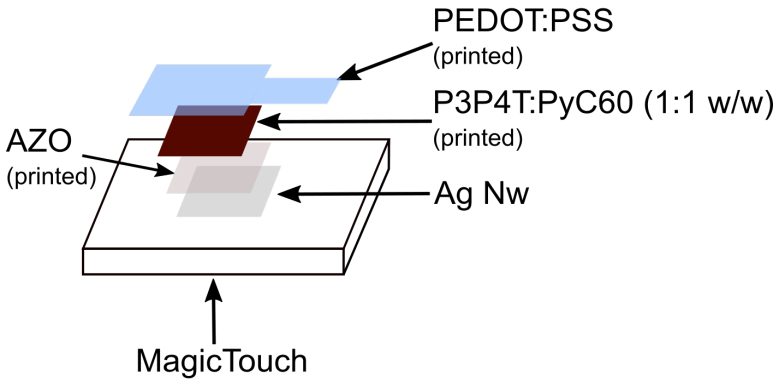

Figure 6.1.: Schematic of assembled printed OPD

[3]combination of AZO and Ag Nw to an electrode
[4]solution of P3HT and ICBA in Toluene (1:1 w/w; 15 mg/ml P3HT/solvent)

6.2. Devices and setups

The different measurement setups are given in Table 6.1. The system for measuring the I/V-characteristic curve is described in subsection 6.2.3.

Table 6.1.: Device list

Device / setup	**Company**	**Model**
Plasma activation	diener electronics	Femto
Spin coater	CHEMAT technology	KW-4A
Inkjet printer	Fujifilm	DMP2850
Thermal evaporator	Balzer Union	MED 010
Profilometer	KLA Tencor	D-500
CAM	KSV Instruments LTD	CAM200
UV/VIS-spectrophotometer	Shimadzu	UV-1800
AFM	nanosurf	easyScan 2
Four-point-measurement	Keithley	2614B SourceMeter
SEM	JEOL	JSM-6490LV
Water purification	Sartorius AG	arium mini plus
LED meter	UPRtek	MK350
Thermal evaporation setup (subsection 6.2.1)		
IR-treatment setup (subsection 6.2.2)		
I/V-characteristic measurement setup (subsection 6.2.3)		

6.2.1. Thermal evaporation setup

Two different evaporation systems were used, where one is commercially available (Balzer Union and listed in Table 6.1) and the other is a self-realised system available at the Institute of Solid State Physics, TU Graz. It is equipped with a 8 l vacuum chamber, rotary vane and turbomolecular pump as well as a quartz crystal microbalance for in-situ tracking of deposited film thickness. This evaporator is used for depositing silver films, while the one from Balzer Union is used for aluminium evaporation.

6.2.2. Infrared(IR)-treatment setup

For drying in-between inkjet printing of layers an infrared setup was used and self-build from a power supply (Voltcraft HPS-13015), a lamp (Osram HLX Xenophot) and a mirror (seen in Figure 6.2). Through the mirror shorter wavelengths will be filtered out as well as a focusing of the light occurs on the printing table, which results in a heating at a temperature of $T \approx 80\,°C$. This can be varied by different focusing or by varying the applied voltage. The IR lamp was mounted in such a way to enable drying

of printed films without removing them from the printing table. As the position of the substrate was not changed no alignment before printing the next layer is necessary.

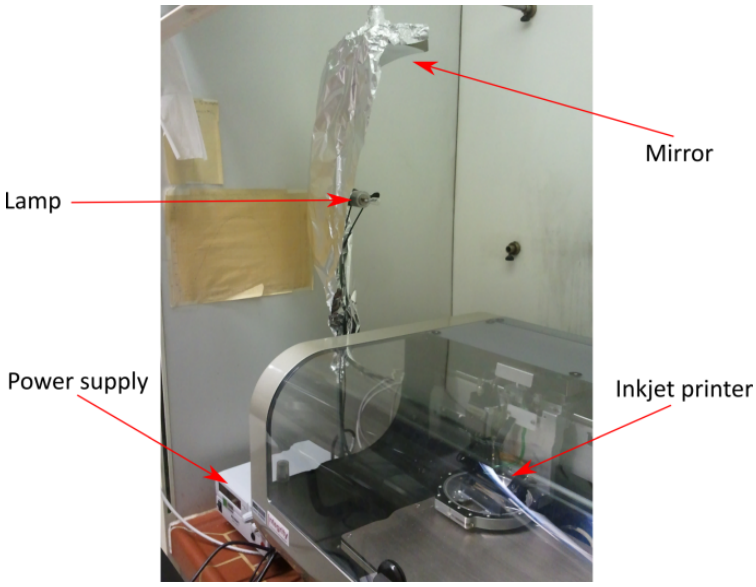

Figure 6.2.: Setup for IR-treatment of printed layers

6.2.3. I/V-characteristic curve measurement setup

In order to measure the current/voltage(I/V)-characteristic curve of an OPD a measurement system was set up with the devices listed in Table 6.2. Figure 6.3b represents the schematic circuit of the system and Figure 6.3a shows an image of it.
The voltage has to be changed manually at the power supply (IPS 2303S from ISO-Tech), while the data collection of the current for a certain voltage occurs for a predetermined number of data points. The amount of data points is set on the multimeter (DMM 4040 from Tektronix).

Table 6.2.: Device list for I/V-characteristic curve measurement

Device	**Company**	**Model**
White LED	CREE XLamp	CMA3090-0000-000R0U0A40*G*
LED driver	MEAN WELL	ELG-100-C1400A
Power supply	ISO-Tech	IPS 2303S
Multimeter	Tektronix	DMM 4040

As a light source a white LED of the type CMA3090-0000-000R0U0A40*G* from CREE XLamp was used. Its spectrum, measured with the LED meter listed in Table 6.1, is given in Figure 6.4.

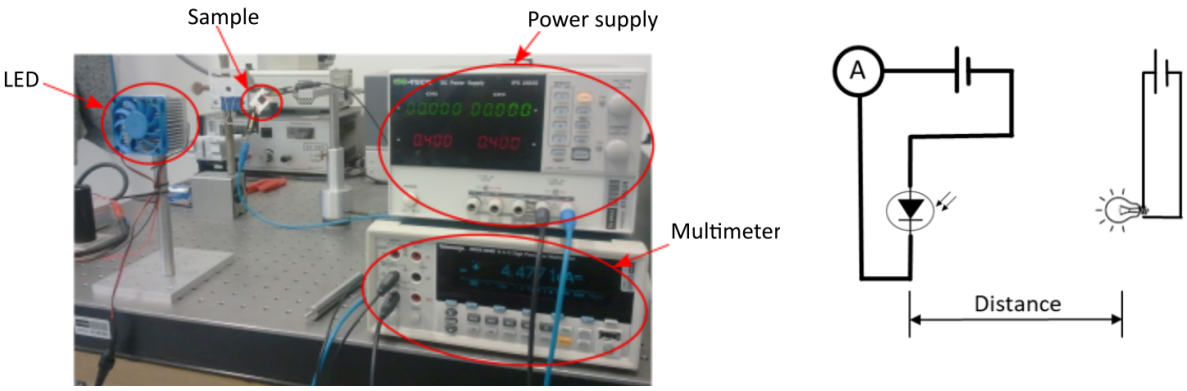

(a) (b)

Figure 6.3.: Setup I/V-characteristic curve measurement
(a): Image of the setup with components
(b): Schematic circuit of the setup

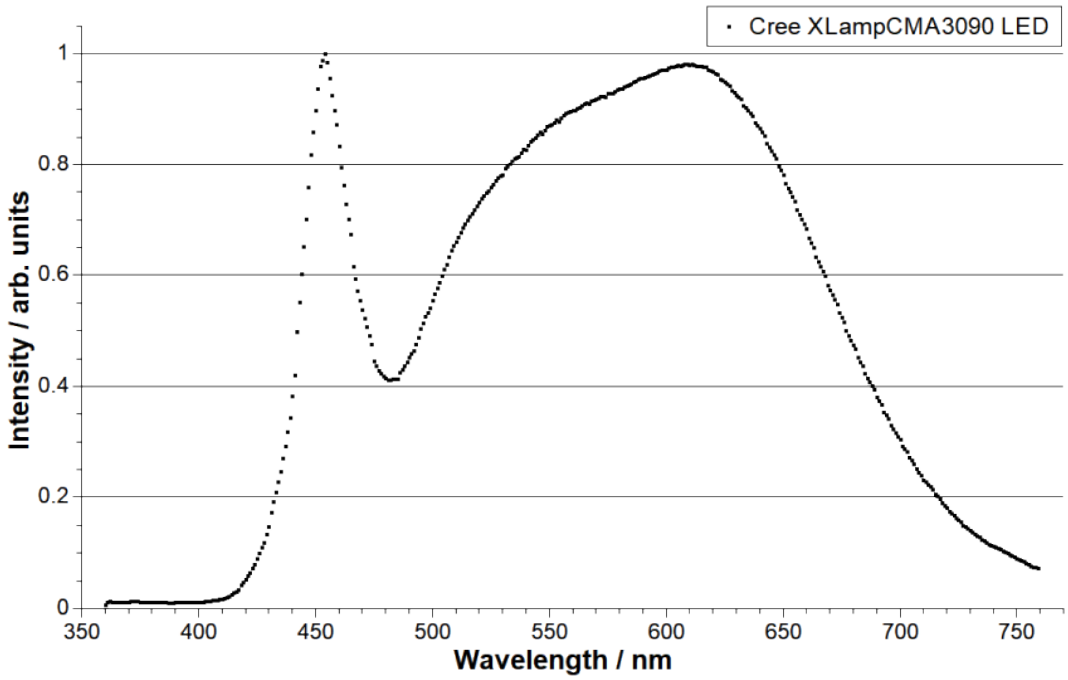

Figure 6.4.: Emission spectra of the white LED

6.3. Experimental methods

This section describes the experimental procedures carried out during characterisation of substrates and deposited films.
Also a short description is given on the fabrication methods.

Profilometry: Thickness, roughness

Thickness and roughness measurements were performed with a stylus profilometer AlphaStep D-500 from KLA Tencor. The profilometer was placed on top of an optical table (from Pörschke GmbH) and an anti-vibration plate from Halcyonics (Micro 40). For characterisation of the polymer substrates three samples each were measured at four positions. In the case of thin films deposited on glass or Si, scratches with tweezers were made to measure the deposited films also in the middle and not just on the edges. The scanned profile length had to be varied depending on the spacing of scratches but was kept constant for the same material and was overall in the range of (0.6 - 0.7) mm and a scan speed of 0.03 mm/s. For the various substrate materials, the height range of the instrument was changed as they exhibit very different thicknesses. An applied force of 2 mg was used for the substrates, while it was reduced when measuring active materials and it will be specified in the following there with the other parameters, for each investigated material.

AFM: Roughness

AFM measurements (easyScan 2 from nanosurf) in tapping mode (tips: PPP-NCLR from NANOSENSORS; resonance frequency: 146 - 236 kHz) were performed on an area of $(10 \times 10)\,\mu$m for the polymer substrate candidates. For the tattoo-papers three samples each at four different positions were measured. The free vibration amplitude varied greatly, so only an example for each substrate candidate will be given in the corresponding section.
AFM images were further analysed with "Gwyddion" software, mainly for correcting artefacts and estimate Roughness R_a.

CAM: Wettability

Contact angle measurements of substrate candidates were done with a CAM200 from KSV Instruments on three samples at three positions. A droplet of distilled water (roughly 0.75 μl) was placed on the investigated substrate with a syringe. Although trials showed no significant impact of slightly different volumes on the contact angle. A more prominent effect was expected through a bigger frame interval, especially for S1-series[5] due to its water-soluble top layer. Varying the frame interval (from 1 s to

[5] Silhouette: one side washed

10 s between frames) was tested and the results are presented in section 7.6. For each frame the contact angle at left and right side of the droplet was determined and then averaged over all positions and samples of the same material. The number of frames was set to 5.

UV/VIS-spectrophotometer: Transmittance, absorbance

In order to record complete UV-VIS spectra of samples and investigate their transmittance in the visible region, relevant for the expected OPD application, a UV-1800 from Shimadzu was used in the wavelength range (350 - 900) nm. Therefore, the examined samples were collected or mounted onto glass slides. A blank reference glass slide was placed in the reference beam path. To fix the glass slides to the sample holder reusable pressure-sensitive adhesive was utilised.

Four-point-measurement: Sheet resistance

The four-point-measurements were carried out with a custom four-point probe setup connected to a Keithley 2602B multifunction sourcemeter, to determine the sheet resistance of deposited materials with the help of Equation 4.3. The tips of the four-point probe are linearly arranged with a spacing of 1.5 mm. A current of few mA were used for the measurements of (10×10) mm samples and varied slightly depending on the sample.
For PEDOT:PSS Equation 4.4 can be used to calculate the conductivity from measured thickness and sheet resistance values.
The sheet resistance was used for comparison of the deposited Ag Nw, as their thickness could not be measured on the tattoo-paper.

Thermal evaporation

Materials (Ag and Al) used during evaporation are listed in Table 5.2 and the setups described in subsection 6.2.1.
The evaporation of Ag occurred at a pressure of $2 \cdot 10^{-3}$ mbar at a rate of 0.5 Å/s observed through a quartz crystal microbalance and a LabView custom monitor interface, starting from Ag pellets (Aldrich, $\geq 99.99\,\%$ trace metals basis).
For aluminium evaporation a MED 010 evaporation system from Balzer was used with a tungsten coil and a wire of Al (umicore, 99.999 %). The wire of Al is given in the tungsten coil and can evaporate when the coil is heated up through a current flow. For this a base pressure of 10^{-4} mbar is used. A physical mask ((10×15) mm), manually done by a thread seal tape, was applied onto the substrate to obtain patterned deposition. After reaching the desired pressure, a slight current was applied, which resulted in a small pressure rise. When the base pressure was reached again, the current is increased until Al vaporises. This can be seen as the glass of the chamber darkens

and after 20 s, to ensure all Al is evaporated, it can be turned off and the system vented.

Plasma activation

For plasma activation the "Femto" plasma system from Diener electronics was used. A weak air plasma (22 W) and a short duration (10 s) at 0.3 mbar was necessary to modifiy the surface energy of MagicTouch, enough to enable good wettability by the PEDOT:PSS ink, as required for obtaining a uniform printed layer.

Spin coating

A KW-4A from CHEMAT technology was used for spin coating of P3HT:ICBA (1:1 w/w). Masking of samples (to pattern the active layer in the form of (11×11) mm was manually done by placing some stripes of Parafilm on top of the printed PEDOT:PSS film ((10×10) mm), completely covering this square area. An excessive amount of liquid was dispensed onto the sample to ensure covering of the whole area before spin coating was carried out at a speed of 800 rpm for 60 s. After removing the mask, the sample was dried and annealed in a oven at 120 °C for 10 min.

Inkjet printing

Inkjet printing of PJet 700, AZO ink and P3P4T:PyC_{60} (1:1 w/w) occurred with a Dimatix Materials Printer DMP2850 from Fujifilm using inks filled in 10 pl cartridges. The used inks, their preparation and processing is given in section 5.2. Although this section provides a more general description about inkjet printing, print parameters of the inks will be given here. How these printed films will look like and other details regarding compatibility will be specified discussing results in their corresponding sections (section 8.1, section 8.2 or section 8.3).

After preparing and filling the inks into a cartridge with a syringe and syringe filter, their print parameters can be investigated. The most important parameters to determine are the jetting wavefunction, tickle frequency, meniscus vacuum and cleaning cycle. Secondarily the jetting voltage can be set for each nozzle individually and it is mainly responsible for the drop velocity.
The form of droplets is mostly determined by the jetting wavefunction, which is the signal sent to piezoelectric actuators. Improper setting of the wavefunction can result in no ejection or spraying, as opposed to the desired droplet formation. The tickle frequency is responsible for keeping the ink in constant motion in order to avoid drying of ink at the air/nozzle interface (and related clogging of nozzle). Cleaning cycles may help against clogging but are also employed when the surrounding of a nozzle has accumulated dirt or drops of ink have formed there. This cleaning can also be done

during the printing process. It should be mentioned that this can result in a high consumption of ink if employed too often or vigorously. For this work cleaning cycles were only necessary before starting to print, as the print areas were rather small.
These are parameters affecting the drop form, size and velocity. Once set only changes in jetting voltages should be made if possible. The inkjet printer has other parameters concerning the printability of inks as, for example, the printhead and ink can be heated to a certain temperature. This was not needed in this thesis but it should be mentioned that there are other parameters that can be set.

Other parameters that are affecting the film properties rather than the shape of droplets per se, are the drop spacing, platen temperature and amount of printed layers. One could also say that these parameters take affect after the droplet has left the nozzle. The drop spacing is related to the spreading of the droplet and therefore the resolution of the printed pattern and is often given in dpi. By manually changing the angle of the printhead the drop spacing is controlled. This is important as a pattern can either be created through the pattern editor or a bitmap and the dpi set there has to coincide with the drop spacing. As the drop spacing is affecting superposition of individual printed droplets, and this is in turn affected by the wettability, the surface properties of the substrate onto which printing occurs are also very important. Therefore, a pre-deposition treatment like plasma activation may be needed.
The plate where the substrate is mounted can be heated and this is given by the platen temperature. This might be important for a homogeneous, smooth surface especially when more than one layer is printed. The applied temperature is limited and will also be employed during printing. This can cause the ink to dry at the nozzles faster and these will clog. To circumvent this a IR-treatment in-between printing of layers can be employed. Here it was only used for PJet 700 and will be specified there.
In Table 6.3 some indications for print parameters of inks used in this thesis are given, as these are depending on the environment. Especially the jetting voltage could be slightly altered by an older cartridge. To keep the temperature in the printer similar even with slight variation of the surrounding temperature the platen temperature was set to 30 °C.

Table 6.3.: Print parameters indication for used inks
JV . . . Jetting voltage
Tf. . . Tickle frequency
MV. . . Meniscus vacuum
T_p . . . Temperature of print plate
Ds. . . Drop spacing
C_c . . . Cleaning cycle employed during printing

Ink	**JV**	**Tf**	**MV**	**T_p**	**Ds**	**C_c**
PJet 700 (PEDOT:PSS)	28 V	5 kHz	4 inches H_2O	30 °C	35 μm	no
P3P4T:PyC_{60} (1:1 w/w)	36 V	5 kHz	3.5 inches H_2O	30 °C	25 μm	no
AZO ink	40 V	1 kHz	5 inches H_2O	30 °C	25 μm	no

Fabrication AZO-electrode

Different drop casting techniques were tested and will be compared in section 8.3. Here a short description is given of the best found solution.
First a layer of AZO ink with a drop spacing of 25 μm was inkjet printed on MagicTouch. No drying was done at this point. A physical mask made of Parafilm was placed manually on the printed AZO layer and Ag Nw were deposited by drop casting in two steps (each 30 μl for (10×10) mm or 45 μl for (10×15) mm) with the aid of a micropipette. After the first deposition the mask was removed and the sample was annealed in an oven at 120 °C for 2 min, a new mask placed and the second step performed. Then the mask removed and annealing repeated at 120 °C for 3 min. For testing an (10×10) mm area was used while for the AZO-electrode an area of (10×15) mm chosen to have a contacting area. A second area also for contacting but of the PEDOT:PSS-electrode was done in the same ratio on a smaller area. The exact size is not as important as it is only for contacting.
This only describes the conducting part of the AZO-electrode. Afterwards AZO is printed for 5 layers with a drop spacing of 25 μm on an area of $(11 \times 11$ mm) and heated in an oven at 120 °C for 10 min. 5 layers were chosen to completely cover the underlying Ag Nw.

I/V-characteristic measurement

All I/V-characteristic measurements were done with the setup described in subsection 6.2.3. In order to compare them better the distance between LED and sample were not changed and neither was the illuminance. The distance was set to 20 cm and the illuminance measured at this position. This was done with a MK350 LED meter from UPRtek three times to yield an average of $(75\,700 \pm 300)$ lx.
Measuring the curve followed the same procedure. At zero bias the measurements were done without the power supply, after connecting the voltage increased. After each change of voltage 30 s were waited before recording 100 datapoints with the multimeter. These 100 datapoints can afterwards be analysed by statistical means. The voltage was increased until a rapid change was observable or further increase of voltage was deemed either not feasible or dangerous for the sample. Before measuring the other direction, the sample was short-circuited to get rid of any possible accumulated charge. Then the voltage again increased, this time in opposite direction.
The dark condition was measured before the illuminated one.

Part III.

Characterisation and results

7. Characterisation of substrate materials

In this chapter the substrate materials, described in section 5.1, are compared regarding some of their properties. Mainly their topography, thickness and transparency are considered, but also their wettability.
The topography and wettability are important for the build-up of the device and future proceedings. Since rough surfaces would probably need an additional smoothing layer and hydrophobic layers further treatment.
Transparency for visible light is required since the light must travel through the polymer substrate to reach the active layer first. The build-up will be in reverse since everything is fabricated on top of the polymer substrate and via transfer will be flipped. An illustration of this will be given in Figure 8.1.

7.1. Preparation for topography investigation

The preparation of the materials depended hugely on the measured quantities and was quite different for the decal transfer tattoo-papers and the medical adhesive. This is mostly because of different transfer methods. The polymer films were transferred onto Si-wafers or cover glass (to record UV/VIS spectra). The surface onto which the films will be deposited is investigated and should therefore face upwards.

Decal transfer tattoo-papers for topography, height and transmittance

For measuring the height and topography of the different decal transfer tattoo-papers (MagicTouch, Silhouette), small samples (cut with scissors) were placed on the surface of distilled water in a vessel at $T = 30\,°C$. The backside part of the paper was placed downwards, and soaked with water which caused the dissolution of the sacrificial layer, sinking the carrier paper and release the transfer layer as a free-standing film floating on the surface of water. After a few minutes these films were "caught" on top of a Si-wafer and dried with an air gun.

As mentioned in section 5.1 the Silhouette tattoo-paper has a water-soluble layer on each side of the polymer film, so they were investigated separately. The S1-series is just floated "normally" since only the sacrificial layer between paper and polymer film should dissolve.
To dissolve both water solvable layers (S2-series[1]) the tattoo-paper is first dragged

[1] Silhouette: both sides washed

with the top side over the water surface for some seconds and then floated. Opposed to the S1-series the film will sink with the paper, but it will only stick to the paper on a few points (mostly edges) as it tends to stay nearly vertical in the water. This is really helpful since catching this film without wrinkling it is not easy. A reasonably well working way is using additional tweezers to "fix" the film on an edge of the wafer and then carefully rise everything simultaneously. Other ways were also tested but were not as efficient.
This technique also has the advantage that it is still possible to identify the top layer throughout the procedure, which is not always given when the film moves freely in water. This is increased by the fact that the film easily slips away from a Si-wafer.
The same method was used for preparing samples to measure the transmittance, recollecting them onto a glass slide.

Medical adhesive for topography, height and transmittance

For the medical adhesive Fixomull another strategy has to be used. If just the height or transmittance is of interest, the adhesive side does not need to be on top. For these measurements its adhesive side is placed in contact with the chosen surface (glass or Si-wafer). In this case the backside (non-adhesive) side will be on top and its surface could be inspected.
To look at the topography of the adhesive side it was glued onto a Si-wafer. This is not ideal, since the polymer film will not be measured independently and the glue's own thickness will affect the measurement. However, after a short examination of the scale of thickness of the medical adhesive ($> 20\,\mu$m) it was deemed acceptable to use glue to attach it onto a Si-wafer. The acrylic glue sheet which is delivered with the MagicTouch decal tattoo-paper was used (was shortly mentioned in section 5.1).

7.2. Profilometer measurements

For the thickness and roughness measurements with the profilometer the samples were prepared as described in section 7.1 with three samples each for the different decal transfer tattoo-papers compositions (MagicTouch, S1-series and S2-series) on Si-wafer. For Fixomull one sample on a Si-wafer and two samples on glass were considered. On each sample four positions (scratches or borders) were measured as described in section 6.3. For Fixomull borders were measured.

In Table 7.1 the results for thickness and roughness are given for the different substrate candidates. MagicTouch is the only one that is smaller than $1\,\mu$m. The thickness of S1-series and S2-series show that the polymer film is around $1.5\,\mu$m and that the water-soluble layer on top of it is twice as big. Fixomull is rather thick compared to the other substrates as it is nearly an order of magnitude larger than S1-series and 60

times larger than MagicTouch.
The roughness R_a can be determined using the profilometer software and was the smallest for MagicTouch ($R_a \approx 50\,\text{nm}$). These are nearly an order of magnitude smaller than the roughness of S1-series and S2-series. Fixomull in these measurements showed a rather large roughness of around $1.8\,\mu\text{m}$.

Table 7.1.: Profilometer measurements of the substrate candidates with 3 samples each and on each sample 4 positions; Number of measurements per substrate kind is 12

Substrate	**Thickness**	**Roughness (raw); R_a**
MagicTouch	$(608 \pm 52)\,\text{nm}$	$(51 \pm 26)\,\text{nm}$
S1-series	$(4\,400 \pm 400)\,\text{nm}$	$(600 \pm 250)\,\text{nm}$
S2-series	$(1\,460 \pm 520)\,\text{nm}$	$(430 \pm 100)\,\text{nm}$
Fixomull-Backside	$(37\,300 \pm 1\,600)\,\text{nm}$	$(1\,800 \pm 600)\,\text{nm}$

For a better understanding representative profilometer measurements of temporary transfer tattoo-papers are shown in Figure 7.1. For Fixomull a graph was omitted because of the big thickness discrepancy.
There are quite significant differences observable. As expected the S2-series is thinner than the S1-series, as the second water-soluble layer was dissolved. Interesting is the fact that the roughness for the raw data of S2-series listed in Table 7.1 is smaller than of S1-series. While this is in principle possible, Figure 7.1 would on first glance suggest otherwise. It has to be said that no waviness was considered and this will be the reason for discrepancy as the curve of S1-series suggest to have one. Since this would be on a $> 100\,\mu\text{m}$-range, it would not affect the on top printed films as much as really sharp, high peaks. The latter should be indeed avoided since, by increasing the number of different films (materials) in the overall multilayer device architecture, they could be the reason for short circuiting.

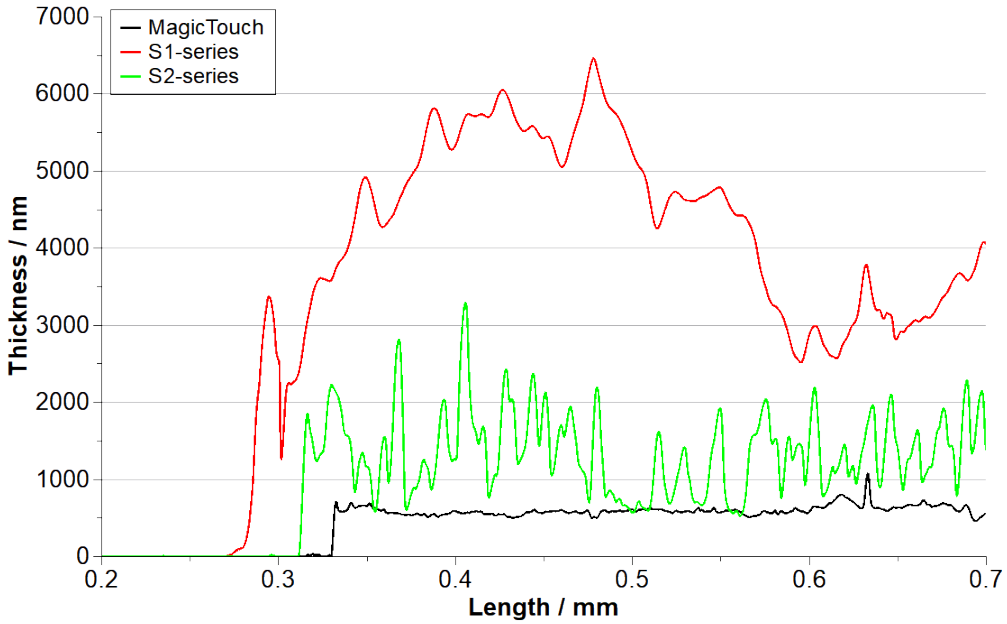

Figure 7.1.: Representative profilometer measurements of different decal temporary transfer papers; black: MagicTouch; red: S1-series; green: S2-series

7.3. AFM measurements

As shortly mentioned in section 7.2 these profilometry roughness measurements where performed on a big scale (>100 μm). To obtain a more detailed topography AFM measurements were performed on an area of 10 μm × 10 μm. While for MagicTouch, S1-series and S2-series the same three samples were used, an alternative had to be considered for Fixomull. One sample on a Si-wafer was investigated to see the roughness of the backside of Fixomull. To measure the front (adhesive) side another sample was prepared so that the adhesive side was on top (as described in section 7.1). Big attractive forces did not allow to measure the surface this way. To circumvent this problem a thin silver film ($t \approx 20$ nm) was thermally evaporated on top and thus suppressing its adhesive properties while hopefully barely affecting its topography.

The roughness is for MagicTouch the smallest among the various substrates, with $R_a = (13 \pm 3)$ nm as compared to Fixomull with Ag-Layer which has $R_a = (25 \pm 20)$ nm, double that of MagicTouch and its uncertainty is comparable to the roughness. Only one Fixomull with Ag-layer sample was measured, but because of its rather lengthy preparation and because Fixomull shows a "milky" transmittance a more detailed analysis was not done at this point. The second reason also holds true for the Fixomull-Backside, which has a roughness of $R_a = (120 \pm 50)$ nm. Investigation of its transmittance will follow in section 7.5. Also S1-series is smoother than S2-series, which is in good comparison to the observed graph in Figure 7.1. S1-series has with $R_a = (44 \pm 23)$ nm

Table 7.2.: AFM roughness measurements of the substrate candidates
N_s ... Number of samples per substrate candidate
N_m ... Number of measured positions per sample
R_a(1st Polynomial) ... Roughness R_a with 1st order polynomial aligned rows

Substrate	**Area size**	$\mathbf{N_s}$	$\mathbf{N_m}$	$\mathbf{R_a}$ **(1st Polynomial)**
MagicTouch	$(10 \times 10)\ \mu$m	3	4	(13 ± 3) nm
S1-series	$(10 \times 10)\ \mu$m	3	4	(44 ± 23) nm
S2-series	$(10 \times 10)\ \mu$m	3	4	(190 ± 50) nm
Fixomull-Backside	$(10 \times 10)\ \mu$m	1	3	(120 ± 50) nm
Fixomull with Ag-Layer ($t \approx 20$ nm)	$(10 \times 10)\ \mu$m	1	3	(25 ± 20) nm

a rather large uncertainty. The roughness of S2-series is nearly five times larger than the one of S1-series.

To give a better impression of the topography, an example for each substrate candidate will be given in Figure 7.2. They have spectral colour schemes so the differences are better visible and it is easier to distinguish between regions with small discrepancies. Also the free vibration amplitude (FVA) is given for each figure.
In Figure 7.2a an example of MagicTouch can be seen. It seems to have a stable ground level with small sized features up to approximately 100 nm. These peculiarities also occur in Fixomull with Ag-Layer (Figure 7.2d).
In Figure 7.2b an example of S1-series is given which is characterised by waviness, similar to what was obtained in the profilometer measurement (Figure 7.1). Nevertheless, they have quite different sizes. S1-series sample does not show sharp features.
In comparison to this Figure 7.2c with a S2-series sample exhibit a rather large roughness up to 1.3 μm. Compared to roughness measurements of the profilometer (Table 7.1) S2-series shows a larger roughness. The change of values is due to the different area sizes considered in the two methods.
For Fixomull the backside (Figure 7.2e) as well as the adhesive side covered with a 20 nm Ag film (Figure 7.2d) were investigated. While the adhesive side covered with an Ag-layer shows a good R_a value (nearly comparable to MagicTouch) the Fixomull-backside shows features as big as nearly 700 nm.

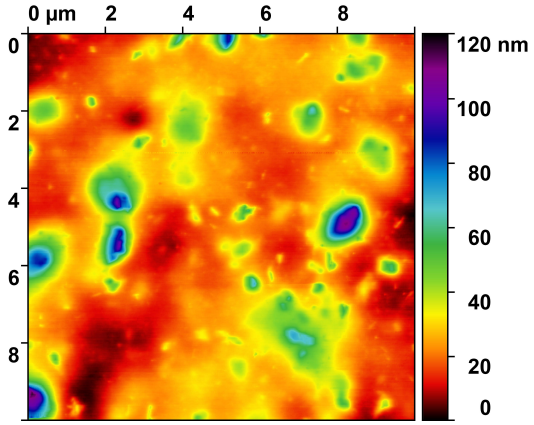

(a) MagicTouch example with FVA = 80, 26 mV

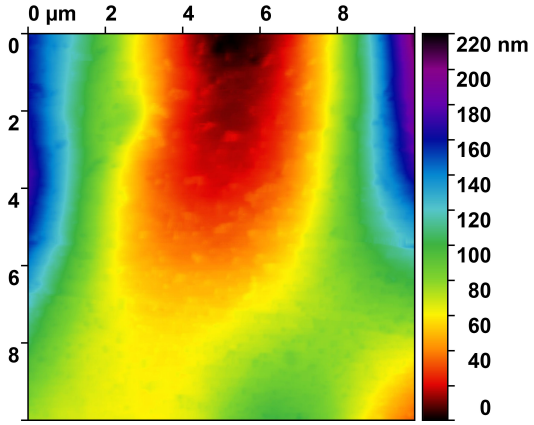

(b) S1-series example with FVA = 190, 1 mV

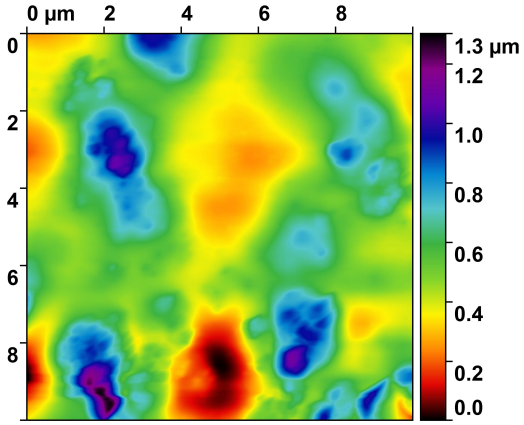

(c) S2-series example with FVA = 601 mV

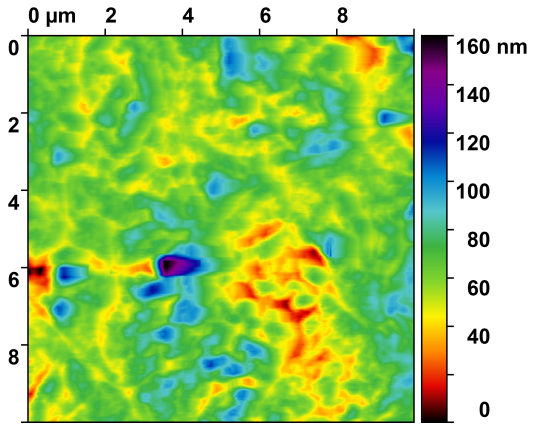

(d) Fixomull with Ag-layer(t ≈ 20 nm); FVA = 120, 1 mV

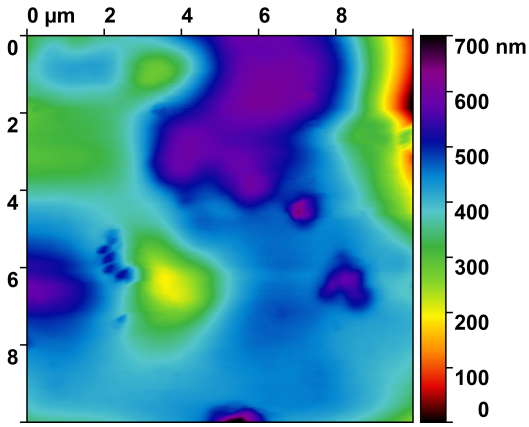

(e) Fixomull-Backside example with FVA = 261, 1 mV

Figure 7.2.: AFM images of substrate candidates after using the software Gwyddion
FVA . . . free vibration amplitude

7.4. Optical microscope

In Figure 7.3 optical microscope images of the various substrate candidates are presented. The samples were the same as for profilometry and AFM and thus mounted onto Si-wafers (described in section 7.1). The images were not taken at a very high magnification (scale bar: 200 μm) to give a better insight in the films homogeneity, also some images tend to be out of focus because of a low depth of focus at higher magnification.
Figure 7.3a is an image of MagicTouch and presents itself quite colourful, which is due to interference. Otherwise no obvious features are visible, except a scratch.
Quite interesting is for S1-series in Figure 7.3b that there seem to be two phases present (bottom left and upper right) and some bigger "bumps" are seen. The presence of two phases is probably due to the fact that the water-soluble layer was partly dissolved. If this is the case one of these should be also observable for S2-series.
Figure 7.3c shows S2-series with scratches for profilometer measurements. It seems to have the same structure as the bottom left corner of S1-series, which confirms the suspicion that S1-series was partly dissolved.
Fixomull with Ag-layer can be seen in Figure 7.3d. Some bigger features are present, while in Figure 7.3e the backside of Fixomull exhibits mostly big features.

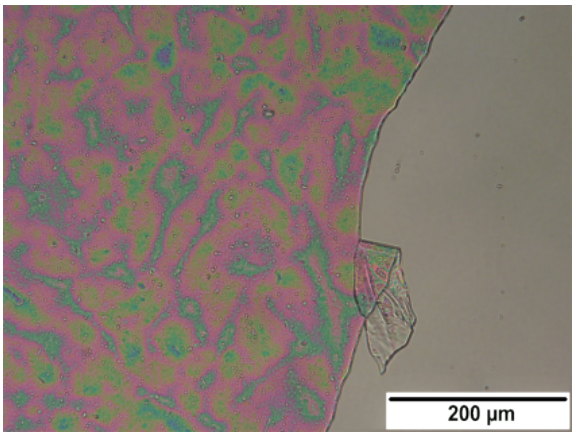

(a) MagicTouch example

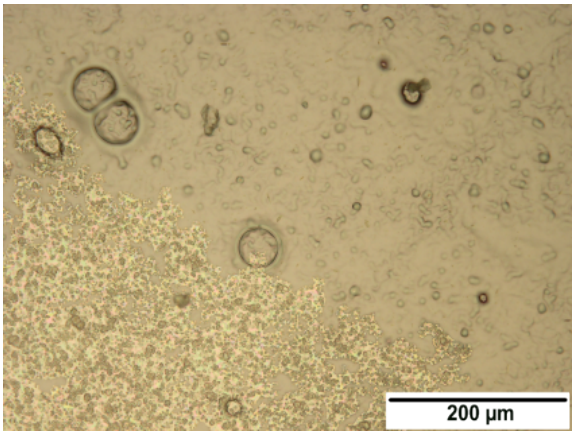

(b) S1-series example

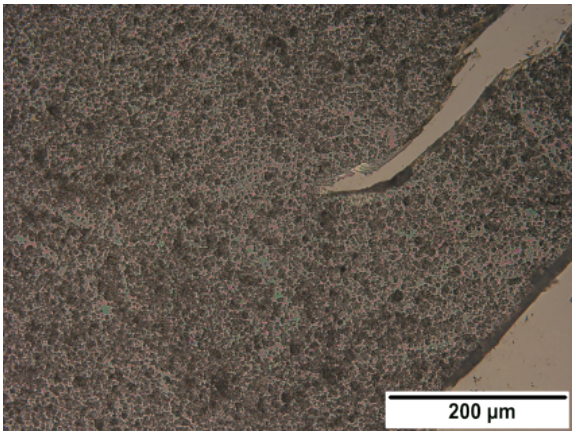

(c) S2-series example

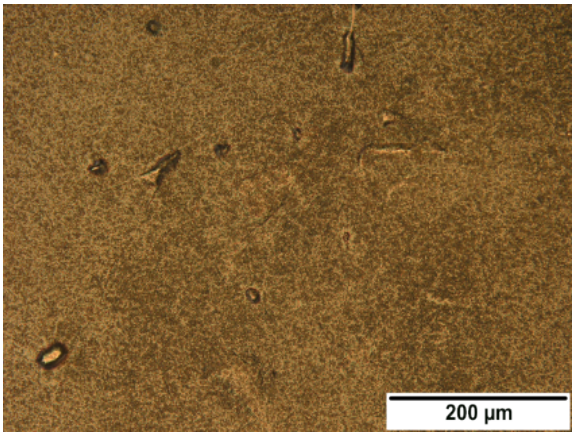

(d) Fixomull with Ag-layer ($t \approx 20\,nm$)

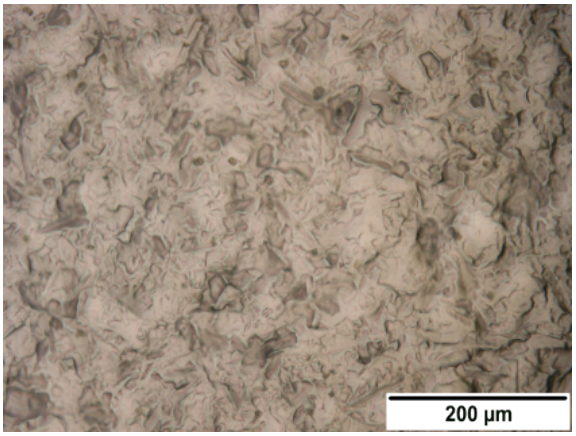

(e) Fixomull-Backside example

Figure 7.3.: Optical microscope pictures of substrate candidates

7.5. UV/VIS-spectrophotometer

For these measurements the samples were attached onto glass slides following the description in section 7.1. S2-series is not considered because of properties observed in previous measurements (thickness, roughness). For better comparison they are all illustrated in one graphic (Figure 7.4). Three samples each are considered for MagicTouch, S1-series and Fixomull and their transmittance measured in the wavelength range from 350 nm to 900 nm.

The spectra of MagicTouch show small discrepancies and are around 100 %, meaning full transparency.
Fixomull-spectra also exhibit very small discrepancies but have a much smaller transmittance of approximately 35 %.
The difference of S1-series samples is quite large (30 - 45) % and can be explained when considering that the water-soluble layer was partially dissolved. By this reasoning this layer of S1-series sample 2 is more damaged than in sample 1. Meaning that sample 2, while reaching a transmittance around 90 %, is more similar to S2-series. The other two samples exhibit only a transmittance of up to 60 % so being quite lower, which would support the theory of the partly dissolved water-soluble layer.

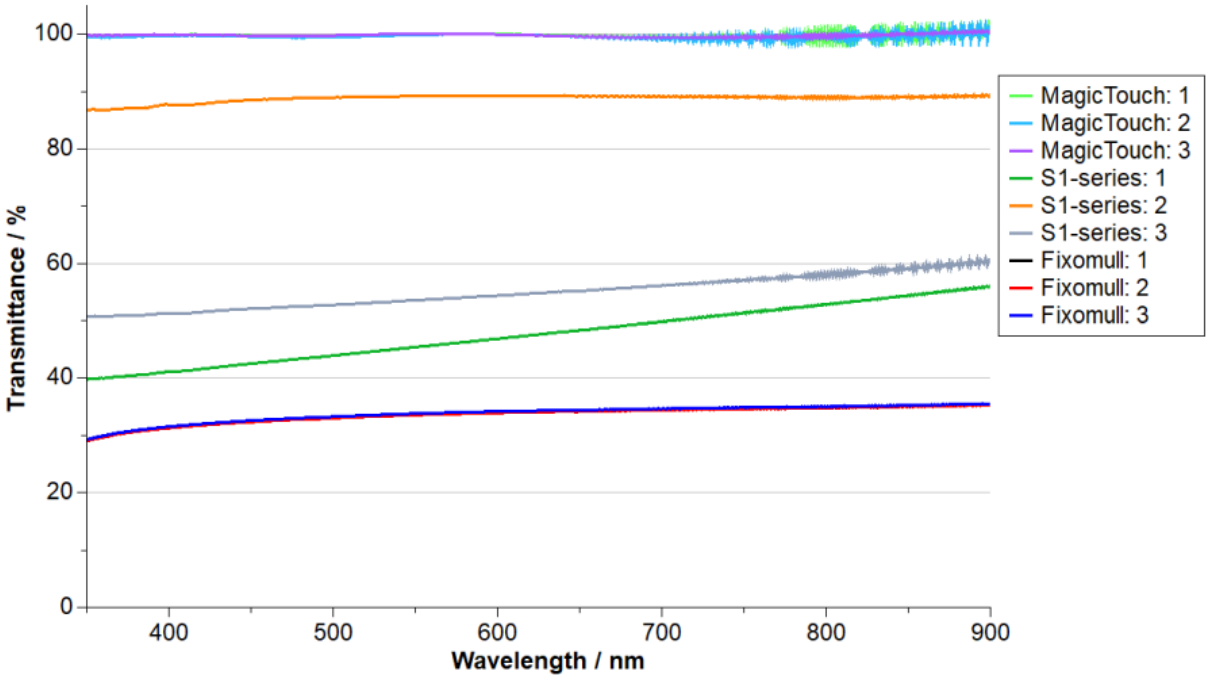

Figure 7.4.: UV/VIS-spectra of various substrate candidates mounted on glass

7.6. CAM

The results of CAM experiments are reported in Table 7.3. They were performed on the samples that were also used for the profilometer measurements. This means the samples were floated in water and collected onto a Si-wafer. Because of that the water-soluble top layer of S1-series, samples could be damaged through water or vapour. Since during printing or other process steps not everything can be controlled it was interesting to see, how this affects the substrate. Differences seem to be observable with an optical microscope and also coincide with UV/VIS-spectrophotometer measurements in section 7.5. So it is expected that also the contact angle will be affected by it.
At this point S2-series was not further investigated as previous investigations (Profilometer, AFM) showed that it is not the best candidate.

Three different samples were considered for MagicTouch and S1-series. On each of these the contact angle was measured at three positions and the deposited volume kept roughly the same.
The effect of varying the frame interval can also be seen in Table 7.3

Table 7.3.: CAM of H_2O on different polymer substrates
N_s ... Number of samples per substrate candidate
N_m ... Number of measured positions per sample
FI... Frame interval
N_F ... Number of Frames
θ_M ... Angle between substrate and liquid, averaged between left and right side

Substrate	$\mathbf{N_s}$	$\mathbf{N_m}$	**FI**	$\mathbf{N_F}$	$\boldsymbol{\theta_M}$
MagicTouch	3	3	1 s	5	$(76 \pm 6)^\circ$
S1-series: sample 1	1	3	1 s	5	$(89 \pm 9)^\circ$
S1-series: sample 2	1	1	1 s	5	$(79 \pm 2)^\circ$
	1	1	5 s	5	$(61 \pm 3)^\circ$
	1	1	10 s	5	$(74 \pm 7)^\circ$
S1-series: sample 3	1	1	1 s	5	$(44 \pm 2)^\circ$
	1	2	10 s	5	$(42 \pm 5)^\circ$
Fixomull-Backside	1	3	3 s	5	$(63 \pm 14)^\circ$

In Table 7.3 three different samples of S1-series and MagicTouch have been distinguished and for some measurements of S1-series the duration of frame intervals changed to see the effect. Samples of S1-series show very different contact angles $\theta_M = (42\text{-}89)^\circ$, which is due to partly dissolution of the water-soluble top layer. The contact angle of the water-soluble layer will be lower than on the underlying polymer.
The effect of frame interval seems to be neglectable, as can be seen either by sample 2 or 3, compared to changes in position or different samples. While the contrast from

the first and second measurement of sample 2 could suggest an effect, the third and measurements from sample 3 indicate that this is resulting from the different position rather than from the frame interval.
Results of MagicTouch ($\theta_M = (76 \pm 6)°$) and Fixomull ($\theta_M = (63 \pm 14)°$) show similar behaviour and not as big discrepancies as S1-series. It was expected that these would show a more hydrophobic nature than S1-series, which was only partly observed. These measurements indicate a hydrophobic behaviour of the polymer substrates and that these might need plasma activation for a proper wetting and formation of a homogeneous film during printing.

8. Build-up, printing and characterisation of deposited layers for an OPD

After considering suitable substrate candidates regarding thickness (section 7.2), roughness (section 7.3), transmittance (section 7.5) and wettability (section 7.6) MagicTouch was selected as the substrate material for the OPD. Its thickness, roughness and transmittance are making it a better choice than the other candidates. These properties are of interest as a thin polymer substrate would be beneficial to conformability and a smooth substrate is desired as an additional smoothing layer is not necessary. The necessity of a transparent substrate is given as after transfer it will be on top. A good wettability is beneficial to achieve a homogeneous film during printing.

The next step was to choose the materials and layout of the photodiode. Two approaches were looked at for the fabrication of the bulk heterojunction. Firstly, fabricating an organic photodiode with common, well established organic materials, no matter the fabrication techniques needed; second, trying to manufacture an inkjet printed OPD with a water-based ink.

Since after the transfer of the OPD onto the target surface the substrate will be on top, the first layer that needs to be deposited is the transparent top electrode. Then the organic bulk heterojunction (active film) follows and lastly the bottom electrode. A schematic of the layered structure, before and after transfer, is provided Figure 8.1.

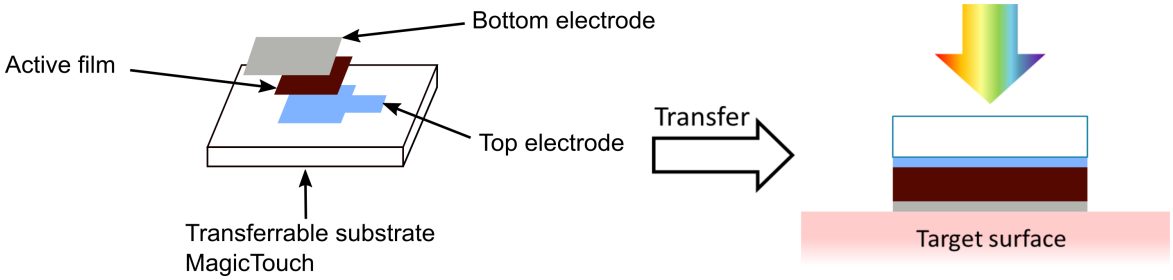

Figure 8.1.: Schematic of build-up and transfer of a transferrable OPD

In the following used materials are described in more detail. This includes their fabrication but also some of their properties. Then in chapter 9 the different layouts are given and their I/V-characteristic curves measured.

8.1. Top electrode: PEDOT:PSS

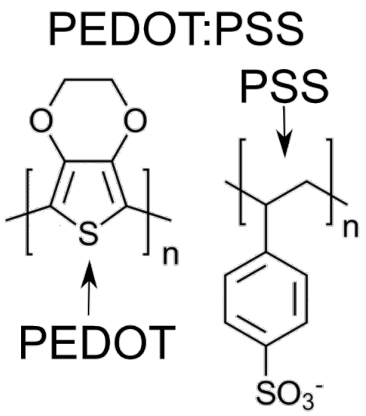

Figure 8.2.: Chemical structure of PEDOT:PSS

Using Poly(3,4-ethylenedioxythiophene) polystyrene sulfonate (PEDOT:PSS) as transparent top electrode is possible due to its semi-transparency and conductivity, which has been improved over the years. This has been achieved through additives or post-treatments for example. [71]
Figure 8.2 shows the chemical structures of the components of PEDOT:PSS, namely Poly(3,4-ethylenedioxythiophene) (PEDOT) and Polystyrene sulfonate (PSS). Here a commercial product called PJet 700 from Heraeus (solid content: 0.6 - 1.2 %) was used.
In order to achieve an uniform printed layer of PEDOT:PSS on MagicTouch it was necessary to use plasma activation. The effect of plasma activation can be seen in Figure 8.3a, whereas Figure 8.3b shows how such a printed film on MagicTouch with plasma activation looks like. For achieving an uniform film a weak air plasma (22 W) and a short duration (10 s) at 0.3 mbar was necessary.
After having obtained a suitable surface activation to attain a homogeneous layer, the printing parameters (drop spacing and number of layers) and curing temperature had to be found. Based on the results of some tests, the parameters were chosen to be printing of two layers with 35 μm drop spacing and an IR-treatment at approximately 80 °C for 3 min after printing of each layer. At the end the samples were annealed in an oven at 120 °C for 10 min. The IR-treatment between layers seemed to improve the film homogeneity, when printing more than one layer. Tests for finding the right parameters were done in collaboration with Alexander Dallinger and effects of drop spacing as well as number of printed layers can be seen in Figure 8.4. More details on this can be found in his Thesis [72].

A test pattern printed with ink PJet 700 and parameters specified above exhibited a thickness of t $\approx$ 60 nm. This was measured on a sample printed on glass and should only be considered an estimate. This estimation permitted to calculate, from sheet resistance measurements carried out with four-point-method (Equation 4.3 and Equation 4.4) on seven samples on MagicTouch, an average conductivity of $\sigma = (670 \pm 110)$ S/cm. This is totally in line with literature values [73] and with manufacturer's specification [70]. Therefore, this is a further confirmation of the formation of a homogeneous, continuous film, having a good superposition among individual printed spots and among printed lines. In Figure 8.5 the UV/VIS-spectrum of PJet 700 is shown for wavelengths from (380 - 900) nm. It has a good transmittance of over 80 % for the visible range. For this measurement PJet 700 was printed on MagicTouch and then the tattoo-paper/PEDOT:PSS was transferred onto glass.

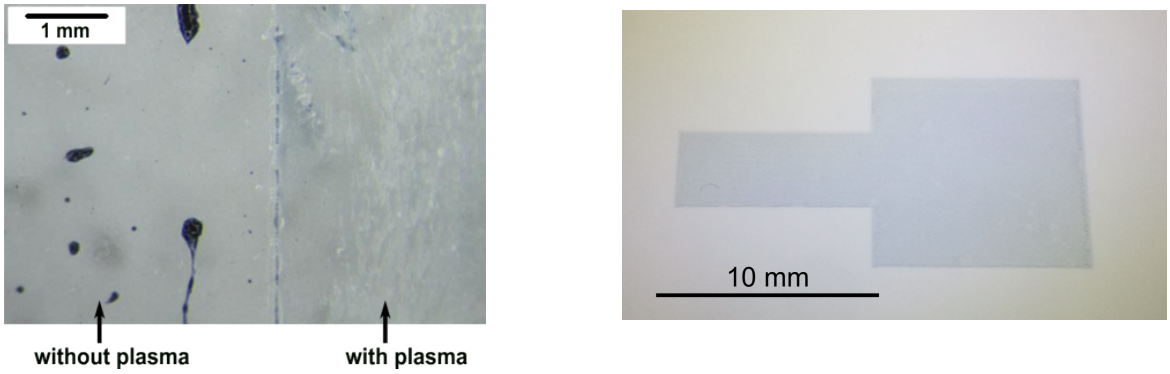

(a) (b)

Figure 8.3.: Printed PEDOT:PSS film
(a): effect of plasma treatment before printing
(b): printed top electrode on MagicTouch with a size of (10×10) mm and a connection for measurements

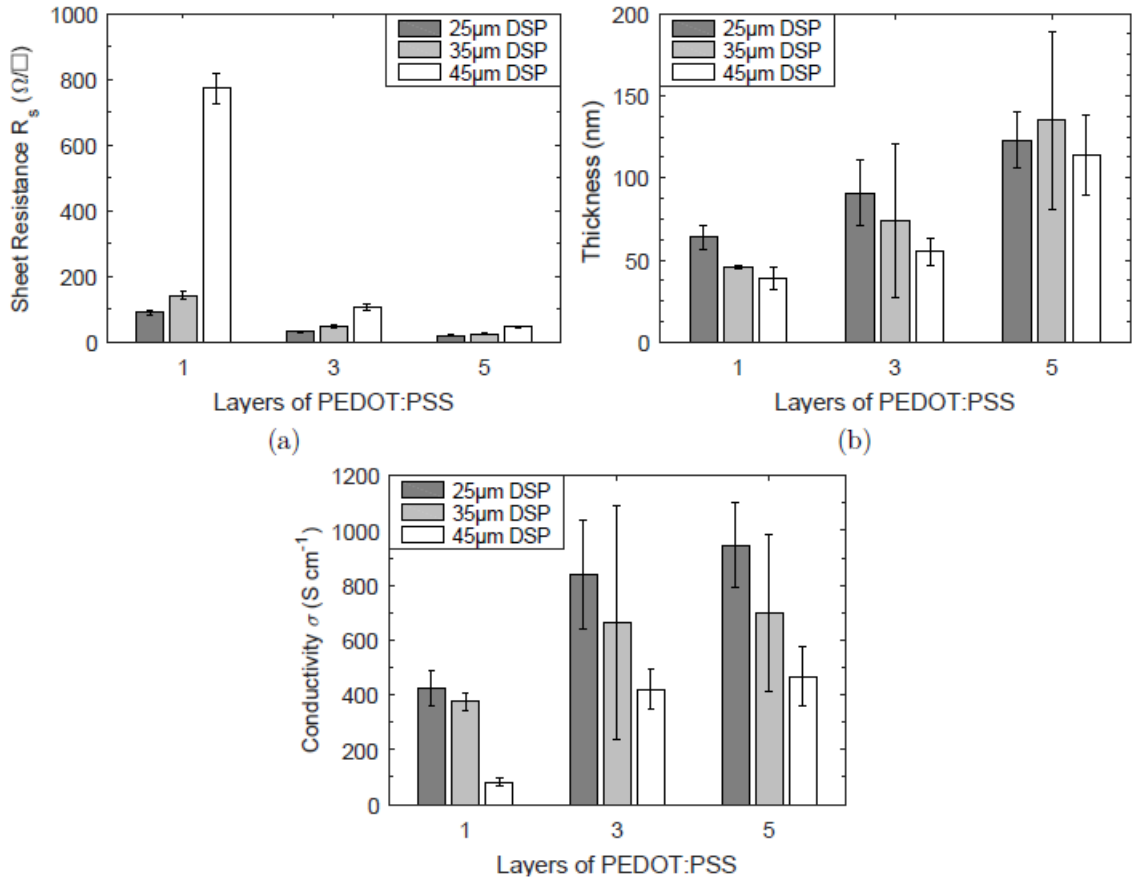

Figure 8.4.: PJet700: sheet resistance, thickness, conductivity with varying drop spacing and number of layers [72]

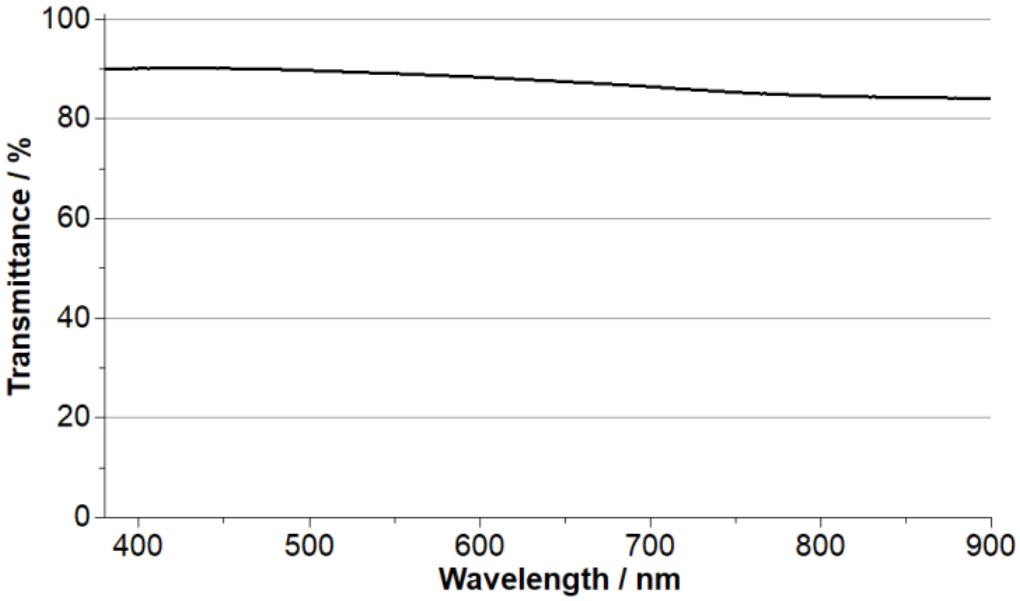

Figure 8.5.: UV/VIS-spectra of printed PJet 700 (PEDOT:PSS) on MagicTouch

8.2. Active film: Polythiophene and Fullerene derivatives

Two cases of polythiophene and fullerene derivative blends need to be distinguished. One is a blend consisting of P3HT and ICBA, a well-known and studied material system, and the other one is based on water-soluble derivatives. Their ink fabrication is given in section 5.2.
Among the water-soluble materials only P3P4T:PyC_{60} (1:1 w/w) was investigated in more detail. P3P7T:PyC_{60} (1:1 w/w)[1] was only very shortly considered in order to get some preliminary data. Films of this material system were obtained by spin coating, in order to investigate a light response in the open-circuit potential, which it showed.

Fabrication of P3HT:ICBA (1:1 w/w) film

The P3HT:ICBA (1:1 w/w) was spin coated and patterned deposition could be performed by manually masking with Parafilm. While this masking is obviously not ideal, it was carried out as an easy, cheap and low effort approach with respect to photolithography or printing.
A thickness analysis with a profilometer on top of the tattoo-paper could not be realised. Therefore, the film thickness and absorption was estimated on a sample prepared by spin coating on glass. The thickness was found to be $t = (230 \pm 40)$ nm when measuring at six positions. The measured length was 1.2 mm, scan speed of 0.1 mm/s and an applied force of 0.8 mg.

Fabrication of P3P4T:PyC_{60} (1:1 w/w) film

The water-based P3P4T:PyC_{60} (1:1 w/w)-solution has the advantage of being inkjet printable. Before printing a plasma treatment analogous as for PEDOT:PSS is necessary on MagicTouch in order to achieve a printed film with good homogeneity. This can be seen in Figure 8.6a. Because of the schematics of the OPD layered structure, this active layer should be printable on top of PEDOT:PSS and MagicTouch surface. Interestingly, if printing of the active layer is carried out shortly after printing of the PEDOT:PSS layer, a plasma treatment would not be needed. While activation by plasma is needed when printing of different layers is carried out on two different days.

Printing parameters included a drop spacing of 25 μm for three consecutive layers with only a short delay of 10 s in-between. After the three layers were printed, the sample was annealed in an oven at 90 °C for 10 min. Cracks were observed when such heat treatment was performed at higher temperatures.
In Figure 8.6b a P3P4T:PyC_{60} (1:1 w/w) film printed on a PEDOT:PSS electrode on MagicTouch is seen. There the edges of the PEDOT:PSS film are completely covered by P3P4T:PyC_{60} (1:1 w/w) to minimise the risk of short-circuiting. Therefore, the active area is slightly larger ((11×11) mm) than the top electrode (PEDOT:PSS),

[1] ink solution of P3P7T and PyC_{60} in 18 MΩ water (1:1 w/w; 6.6̇ mg/ml P3P7T/water)

which has the same shape and size as seen in Figure 8.3b.

Again a film on glass was printed so that a comparison with P3HT:ICBA (1:1 w/w) could be done. Thickness measurements (profilometer, scan length: 0.7 mm, scan speed: 0.03 mm/s, force: 1 mg) on ten positions resulted in $t = (260 \pm 30)$ nm. Printing on glass resulted in some waviness as printed lines overlap (Figure 8.7). When printed on MagicTouch this can only be seen with one layer (Figure 8.6a) and mostly will be smoothed out as seen in Figure 8.6b when more layers are printed on top. This was deemed satisfactory, but might be optimised further.

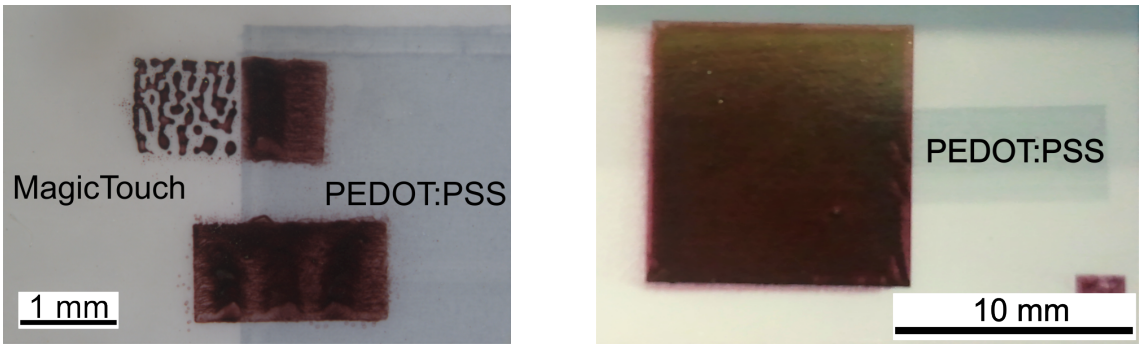

(a) (b)

Figure 8.6.: Printing of water-soluble P3P4T:PyC_{60} (1:1 w/w)
(a): printed layer without (top) and with (bottom) plasma treatment
(b): complete device with 3 layers printed on PEDOT:PSS and MagicTouch

Although PJet 700 is a waterborne dispersion, the PEDOT:PSS film is not damaged by the further deposition of water-based P3P4T:PyC_{60} (1:1 w/w) ink. In general, it has been observed that PEDOT:PSS is hardly affected by water after it has dried and properly annealed. Effects of heat treatment on PEDOT:PSS are for example described in [74, 75].
In contrast to this the P3P4T:PyC_{60} (1:1 w/w) film could be easily damaged by water and thus some precautions should be taken during transfer of the tattoo. Together with water, the film is also easily damaged by isopropanol, as shown in Figure 8.9.

Comparison P3HT:ICBA (1:1 w/w) and P3P4T:PyC_{60} (1:1 w/w)

In order to compare these two blends, one sample each were prepared on glass so that their absorbance could be investigated. An optical microscope image of them can be seen in Figure 8.7. There millimetre-paper was used as a background and can be seen in the P3HT:ICBA (1:1 w/w) part. Printing of P3P4T:PyC_{60} (1:1 w/w) on glass is not ideal as the achieved film is not perfectly homogeneous, as shown in Figure 8.7 with brighter spots in this part. In the glass part the millimetre-paper is not recognisable because of high illumination and its reflectance. Here it seems that the P3P4T:PyC_{60} (1:1 w/w) absorbs more than P3HT:ICBA (1:1 w/w), as the background

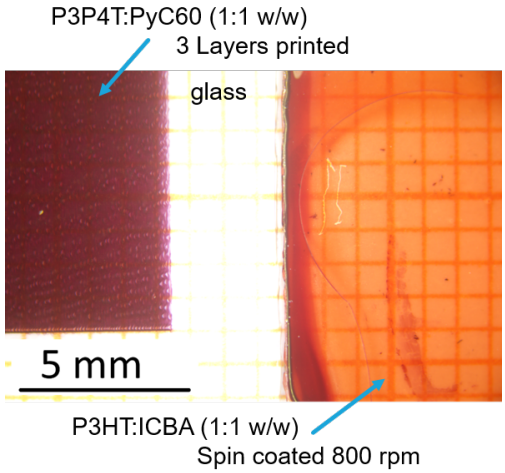

Figure 8.7.: Image-comparison of samples with different polythiophene and fullerene derivatives

can only be seen in the P3HT:ICBA (1:1 w/w) region.
In Figure 8.8 the UV/VIS-spectra from (250 - 900) nm are given. There also the thickness of both films are indicated and they are comparable. Noticeable is a difference of the max. absorbance peak (P3HT:ICBA (1:1 w/w): $\sim$ 480 nm; P3P4T:PyC$_{60}$ (1:1 w/w): $\sim$ 530 nm). For higher wavelengths ($>$ 700 nm) the absorbance drops to nearly zero for P3HT:ICBA (1:1 w/w) and P3P4T:PyC$_{60}$ (1:1 w/w) is slightly higher but also dropping.

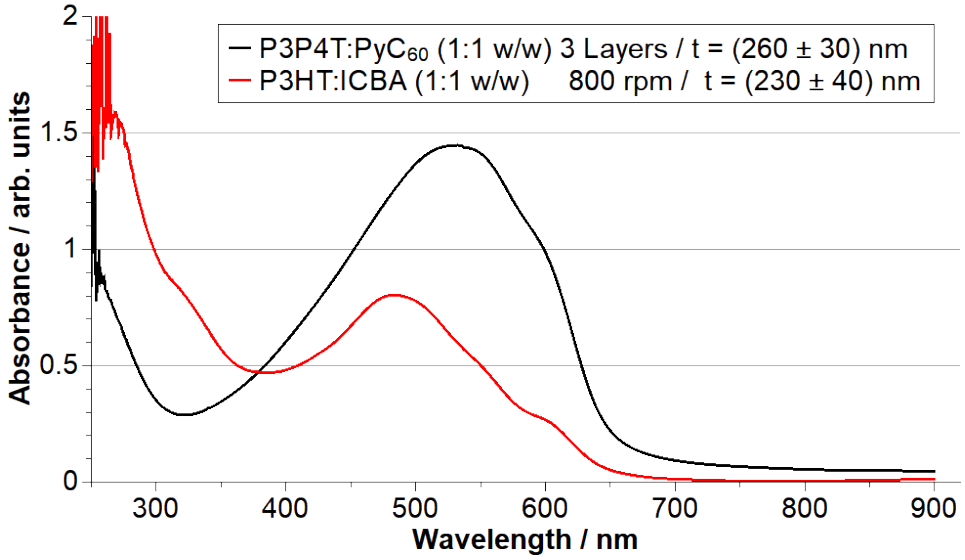

Figure 8.8.: UV/VIS-spectra comparison of spin coated P3HT:ICBA (1:1 w/w) and printed P3P4T:PyC$_{60}$ (1:1 w/w)

8.3. Bottom electrode: Aluminium(Al) or second transparent electrode

As shortly mentioned in Methodology (section 6.1) a printable reactive silver-ink was first tested. It was a commercial product (Silver complex ink) from Electroninks Inc., which is similar to the one used in [76]. As this resulted in short-circuiting of the device other approaches for the electrode were considered.
Two possibilities were considered as regards to the materials for having a bottom electrode, namely physical vapour deposited Al and AZO/ Ag Nw (AZO-electrode). For layouts using a AZO-electrode, a second semi-transparent electrode, would grant the photodiode to be operated from both sides and thus enhance the application possibilities. As one of the goals of the present project would be to investigate strategies for achieving a fully printed OPD, the second option would be preferable, as it allows a vacuum-free fabrication process.

Evaporation of Al

Due to the used setup, which was not integrating a quartz crystal microbalance, no real in-situ control over the thickness of the deposited film was possible during the deposition. In order to get an estimate of the thickness a glass substrate was put in the chamber next to one of the samples. Afterwards, thickness of deposited Al was measured at ten positions with a stylus profilometer (scan length: 1 mm, speed: 0.1 mm/s, force: 5 mg) and resulted in $t = (79 \pm 4)$ nm. As long as the film is not so thick that it hinders the transfer process and has good conductivity, it is acceptable.

First considerations about deposited Al included compatibility with the tattoo-substrate, its transferability and the underlying films. Tests showed that these are not problematic and even after its transfer no cracks were observed.

Ag Nw and AZO electrode

In order to use vacuum-free fabrication methods a combination of Ag Nw and AZO was utilised and is therefore named "AZO-electrode". At first the idea was to use just the AZO ink to have a second inkjet printed, semi-transparent electrode. Due to its bad conductivity the combination with Ag Nw was considered.

AZO acts as an electron transport layer, is inkjet printable and has a nominal visible light transmittance of over 90 % [77]. The inclusion of AZO should reduce the dark current and therefore improve the device performance.
Ag Nw on the other hand allow for a flexible, transparent electrode with good conductivity. While their size is not suitable for inkjet printing, other simple manufacturing processes such as spin coating, drop casting or spray coating can be utilised. Patterning was again achieved through manually masking with Parafilm.
In Figure 8.9 it can be seen that while drop casting Ag Nw the water-soluble active

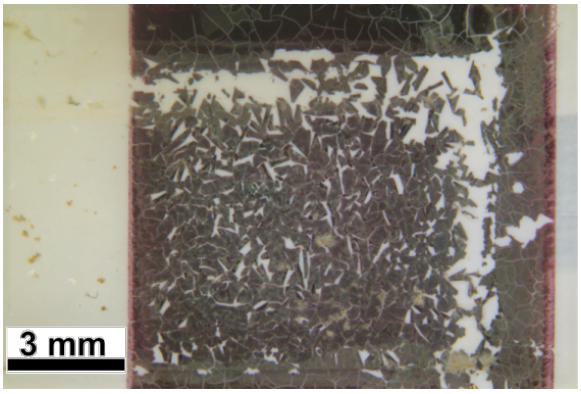

Figure 8.9.: Incompatibility of AZO-electrode and printed P3P4T:PyC_{60} (1:1 w/w) film

layer is damaged. For this sample AZO was printed on P3P4T:PyC_{60} (1:1 w/w) and PJet 700 and afterwards the Ag Nw were deposited. The most damage was done at the edges of the masking and this manifested itself as large stripe-like white areas with a few islands located in them. To circumvent this problem, the AZO-electrode was fabricated on a second MagicTouch tattoo-paper substrate and afterwards through lamination both parts combined. This is only necessary for the AZO-electrode and how this layout looks like is shown in section 9.3.

First trials showed that the Ag Nw do not show good conductivity ($> 5\,\mathrm{M\Omega}$) when spin coated, therefore drop casting was chosen as an alternative.

Conductivity Ag Nw - Drop casting

To achieve good conductivity different deposition techniques were tested. Table 8.1 shows the sheet resistance of some of these tests. Drop casting of 60 μl Ag Nw either directly or after inkjet printing of one layer of AZO (25 μm drop spacing) resulted in a sheet resistance of around $200\,\Omega/\square$ but the uncertainty is nearly as big. The resistance can be lowered by dividing the drop casting into two steps and performing the first before drying the AZO film.
In this way the sheet resistance was lowered to $R_s = (12.4 \pm 5.1)\,\Omega/\square$, a good improvement. Since cluster and agglomeration were visible and the distribution of Ag Nw uncertain, a sample was examined with a SEM (JOEL JSM-6490LV) with an acceleration voltage of 10 kV.
SEM images are reported in Figure 8.10, where Figure 8.10a is an overview. Areas with different surface densities of Ag Nw were observed across the film. It is quite clear that while it is not homogeneous, a mesh of interconnected nanowires is present. In Figure 8.10b a detailed view of Ag Nw is given, with multiple Ag Nws piling up and in contact with each other.
The relative high resistivity can be probably ascribed to both the local low density of nanowires and a large contact resistance between them. It was also observed that the

Table 8.1.: Sheet resistance of different deposition techniques of Ag Nw on MagicTouch
N_s ... Number of samples
N_p ... Number of measured positions per sample
R_s ... Sheet resistance with linear four-point-probe

Deposition technique	$\mathbf{N_s}$	$\mathbf{N_p}$	$\mathbf{R_s}$ **in** $\Omega/\square$
Drop casting 60 μl Ag Nw on (10×10) mm	3	1	157 ± 192
1 Layer AZO [120 °C, 2 min] + drop casting 60 μl Ag Nw [120 °C, 3 min] on (10×10) mm	4	4	230 ± 170
1 Layer AZO + drop casting 30 μl Ag Nw [120 °C, 2 min] + drop casting 30 μl Ag Nw [120 °C, 2 min] on (10×10) mm	2	3	12.4 ± 5.1

way of contacting makes a big difference in resistance measurements. Broader stripe-like flat contacts worked better than tip-like ones, as the contacting area is bigger. This type of contacts were realised with copper foil for instance.

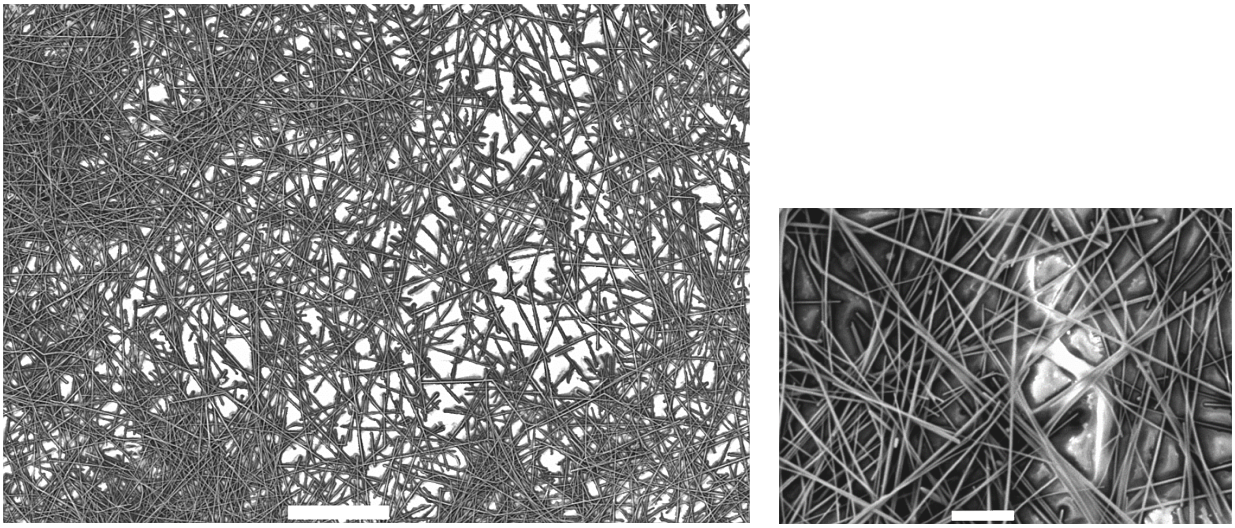

(a) (b)

Figure 8.10.: SEM images of Ag Nw
(a): overview; scale bar = 50 μm
(b): zoomed in; scale bar = 5 μm

After depositing Ag Nw, printing of AZO concludes the fabrication of AZO-electrode. Therefore, five layers of AZO were printed to ensure covering of the Ag Nw. In Figure 8.11 an image of this AZO-electrode can be seen. The printed AZO on Ag Nw looks a little reddish there and is indicated. Furthermore, the contact areas for both electrodes are marked. As the MagicTouch/P3P4T:PyC_{60} (1:1 w/w) part will be laminated on

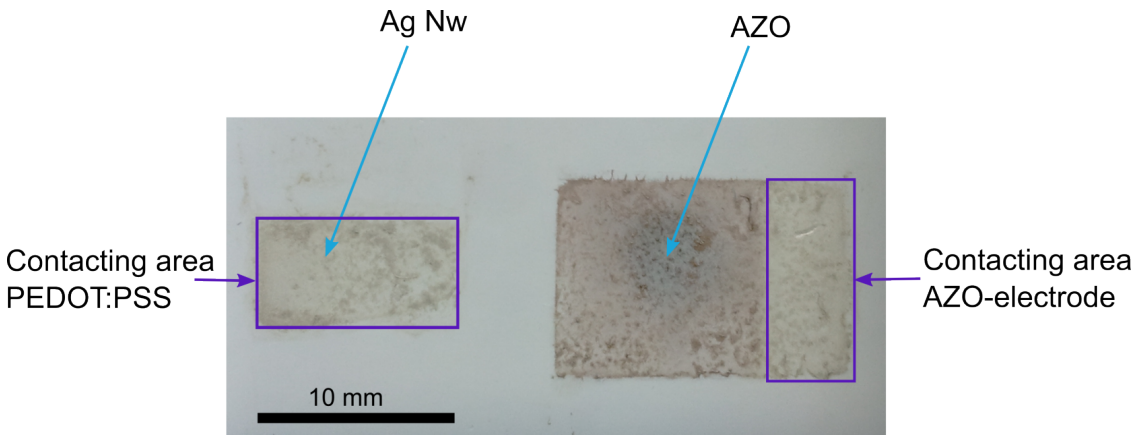

Figure 8.11.: AZO-electrode on MagicTouch

top of the MagicTouch/ AZO-electrode part, a patterned interconnector was made in order to enable contact. This was also fabricated with Ag Nw.

A UV/VIS spectrum of the AZO-electrode was taken. To this purpose an electrode was fabricated on MagicTouch and transferred onto glass with glue. Transferring the AZO-electrode without glue often resulted in cracks. The acrylic glue that comes with MagicTouch was used. The spectra of such an electrode with acrylic glue can be seen in Figure 8.12. Over the wavelengths of (380 - 900) nm this spectrum is in the range of (40 - 60) %.

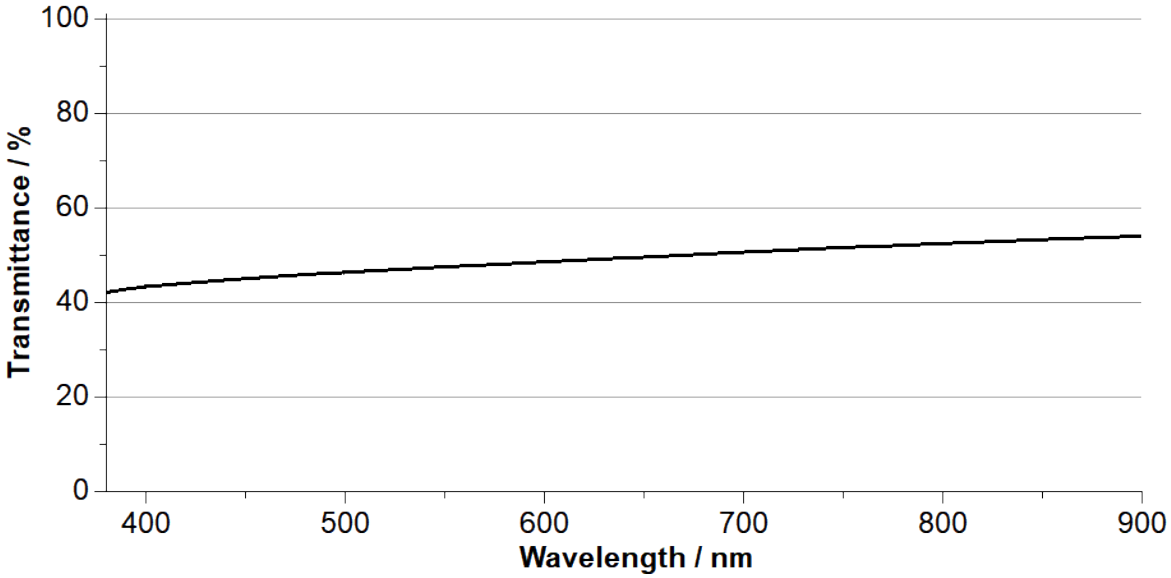

Figure 8.12.: UV/VIS-spectra of AZO-electrode on MagicTouch with acrylic glue

9. Characterisation of the OPD

For initial testing of the OPD the photo-response of the open-circuit potential was looked at, for determining the presence of photo-sensitivity. In order to determine a photodiode behaviour, I/V-characteristic measurements were performed. Figure of merits were not measured as the performance parameters were not as important as the functionality at this initial stage of development.
All samples use PEDOT:PSS for a top electrode as outlined in section 8.1. Three cases are looked at separately in the following. Namely:

- PEDOT:PSS/P3HT:ICBA (1:1 w/w)/Al on MagicTouch
- PEDOT:PSS/P3P4T:PyC_{60} (1:1 w/w)/Al on glass
- PEDOT:PSS/P3P4T:PyC_{60} (1:1 w/w)/AZO-electrode on MagicTouch

While measuring an I/V-characterising curve, a setup with a xenon arc lamp was damaged and a new one was realised with a white LED as described in subsection 6.2.3. This took some time and delayed the measurement of samples. Moreover, due to a shortage in materials all samples could not be reproduced.
Due to manual masking during fabrication, current instead of current-density is used for the plots, although the targeted area size was always maintained at approximately $1\,cm^2$.

Samples on MagicTouch with an evaporated Al electrode have been illuminated through the substrate (MagicTouch still on back-paper) before the transfer. For these samples indeed a measurement before transfer would not have been possible because of a lack of transparency of the Al electrode.

9.1. PEDOT:PSS/P3HT:ICBA/Al

In Figure 9.1 a schematic layout of P3HT:ICBA (1:1 w/w) with evaporated Al is shown. Therefore, the active film is spin coated and an Al film evaporated. The fabrication steps for the different films are given in chapter 8.
One sample was measured and transferred onto glass six months after fabrication. A second measurement was performed within 48 h after transfer and a third three weeks after transfer. During transfer the contacts were partially damaged and had to be fixed with silver epoxy.
The I/V-characteristic curve of this sample can be seen in Figure 9.2, where for better comparison all curves before and after transfer are plotted. Both ID (dark current, no illumination) and IL (photo-current, during illumination with LED) are shown for comparison for each test performed with the sample. The black and red curves are for

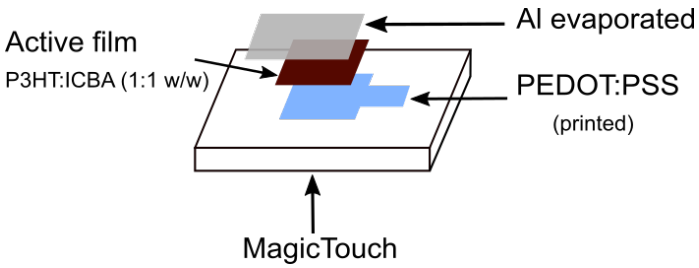

Figure 9.1.: Build-up of OPD with P3HT:ICBA (1:1 w/w)

the same sample still supported on paper before the transfer. Even after six months since fabrication a photodiode behaviour can be seen clearly, as in forward direction a current flows while in reverse bias the current is enhanced when the photodiode is illuminated. Photo-sensitivity was retained, although it has been affected by ageing. Indeed, the photo-response only really starts after applying a negative voltage.

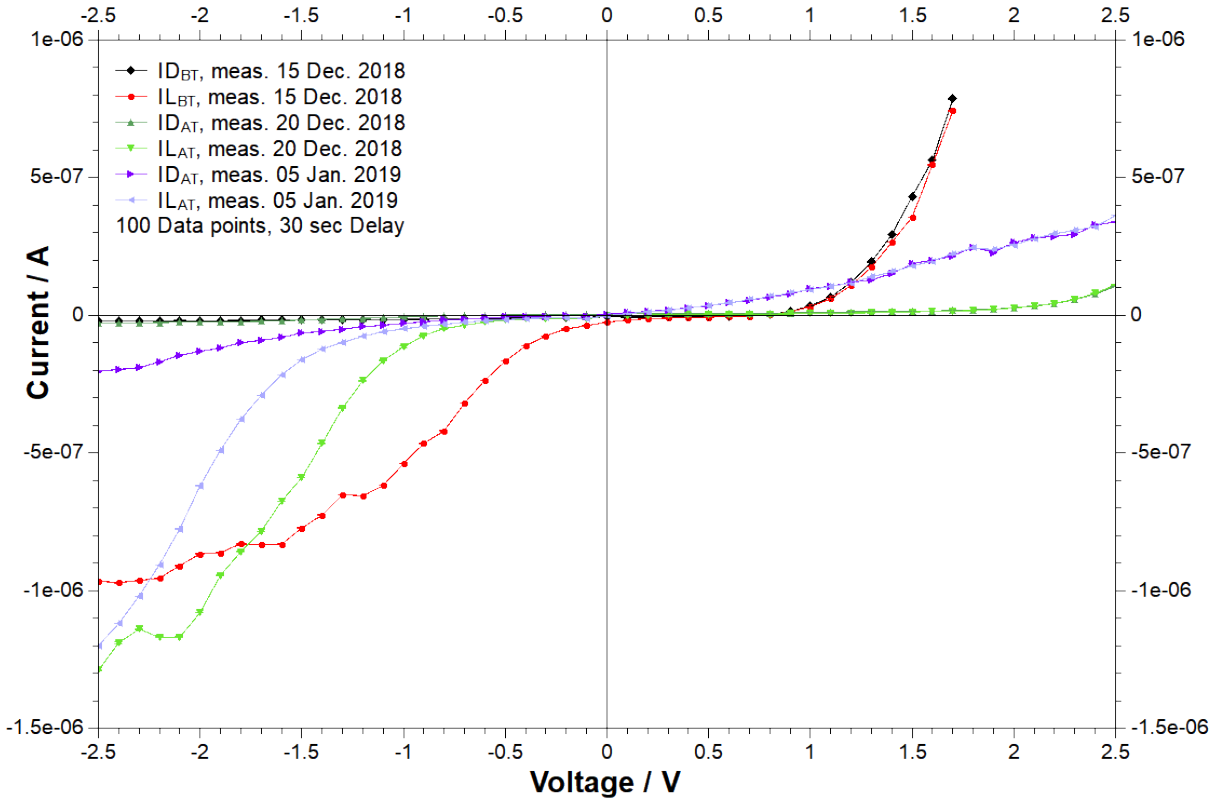

Figure 9.2.: I/V-curve 1st sample PEDOT:PSS/P3HT:ICBA (1:1 w/w)/Al; Fabricated: 08 June 2018
ID... Dark current IL... Current with LED, illuminance: (75 700 ± 300) lx
The indices BT and AT indicate if it was measured before (BT) or after (AT) transfer.

The dark and light green curves have been taken within 48 h after transfer. In forward direction the current flow started later than before the transfer. Again a photodiode

behaviour is observable as under reverse bias one can clearly distinguish between dark and illuminated current. Measuring the same sample three weeks later resulted in the dark and light purple curves. There an applied negative voltage still allowed for distinguishing between dark and illuminated current, although the dark current was higher than for the other measurements.
So in all three cases one can distinguish the curves with and without illumination, but their behaviour slightly differs. Evidently in forward direction the curves after transfer showed a lower current. Not as drastically were the differences under negative bias. The lower current with illumination before (red curve) compared to after (bright green and purple) the transfer is due to the fact that before transfer the sample had to be illuminated through the back-paper.

In Figure 9.3 the I/V-curves of a second sample with the same layout can be seen. In this case the sample was measured for the first time (before transfer) on the same day of fabrication. It was then transferred onto glass and measured three days after fabrication. A third measurement was carried out three weeks later.

These three measurements on the same sample are summarized in Figure 9.3a and Figure 9.3b.

- Before transfer, same day as fabrication: black (ID) and red (IL) curve
- After transfer, three days after fabrication: dark green (ID) and light green (IL) curve
- After transfer, three weeks after fabrication: dark purple (ID) and light purple (IL) curve

All three cases showed a good photodiode behaviour with a low dark current under an applied negative voltage and a current flow in forward direction. When the sample was illuminated, a current was also flowing when applying a negative voltage.

One thing that was noticeable was the higher current (-25 μA) compared to the first sample seen in Figure 9.2. Moreover after transfer the values were nearly an order of magnitude smaller than before, a feature which was not observed in the first sample. A plausible cause for this behaviour is that the second sample was damaged during transfer.
Both samples showed a decrease in current in forward direction after transfer.

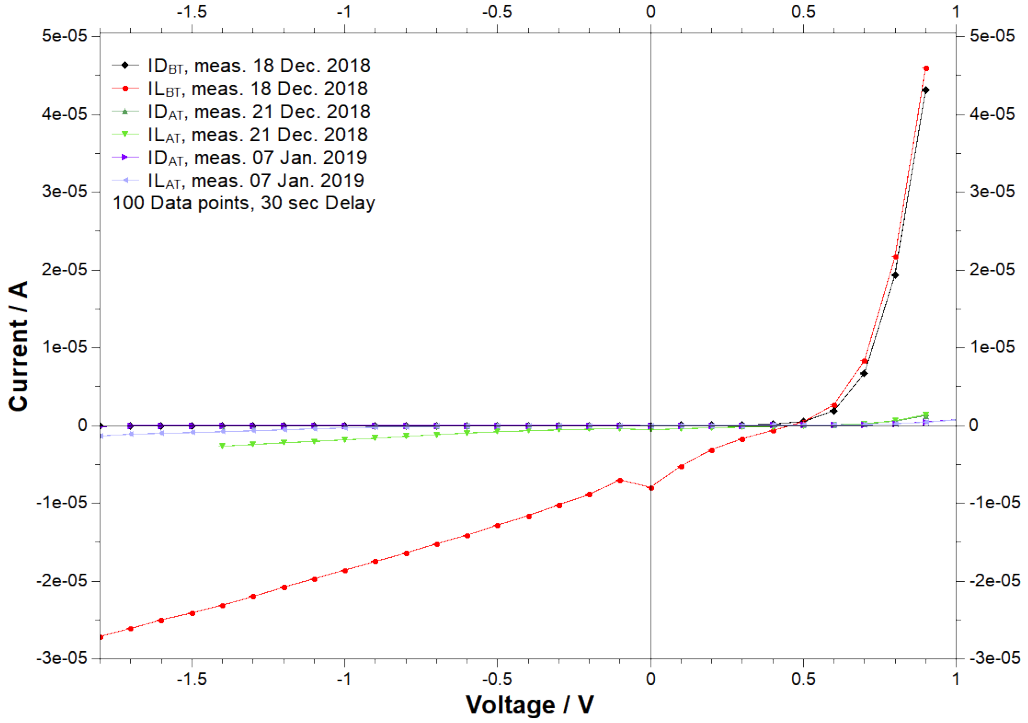

(a) Second sample

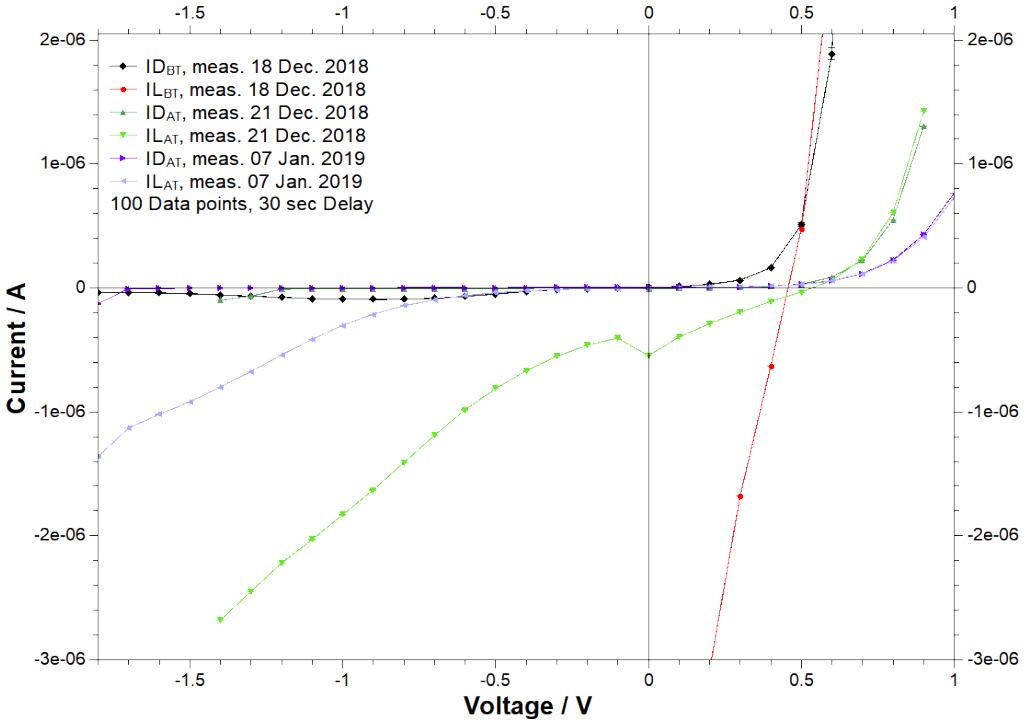

(b) Second sample, zoomed in

Figure 9.3.: I/V-curve 2nd sample PEDOT:PSS/P3HT:ICBA (1:1 w/w)/Al; Fabricated: 18 Dec. 2018
ID... Dark current IL... Current with LED, illuminance: (75 700 ± 300) lx
The indices BT and AT indicate if it was measured before (BT) or after (AT) transfer.

9.2. PEDOT:PSS/P3P4T:PyC$_{60}$/Al

A sample with the new water-soluble blend (P3P4T:PyC$_{60}$ (1:1 w/w)) on glass and with Al as an electrode was prepared and then measured over six months later. This layout with a printed active film of P3P4T:PyC$_{60}$ (1:1 w/w) is illustrated in Figure 9.4.

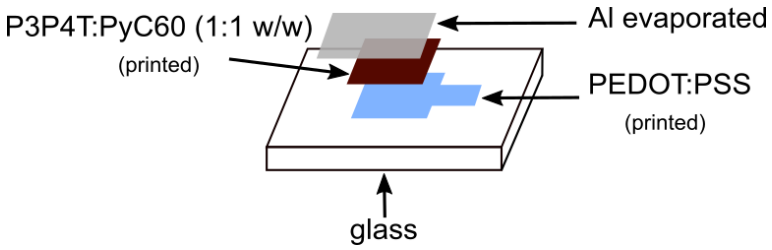

Figure 9.4.: Build-up of OPD with P3P4T:PyC$_{60}$ (1:1 w/w)

In Figure 9.5 the I/V-measurement of a sample is given. The sample was measured six months after its fabrication. Again a diode behaviour was observed, but the device did not work as a photodiode, as the dark and illuminated curves can barely be distinguished. Only a slight photo-response is maybe recognizable for voltages lower than -2 V, although a concomitant rise of dark current is observed.
Due to age and degradation the behaviour of this sample will have been worsened.

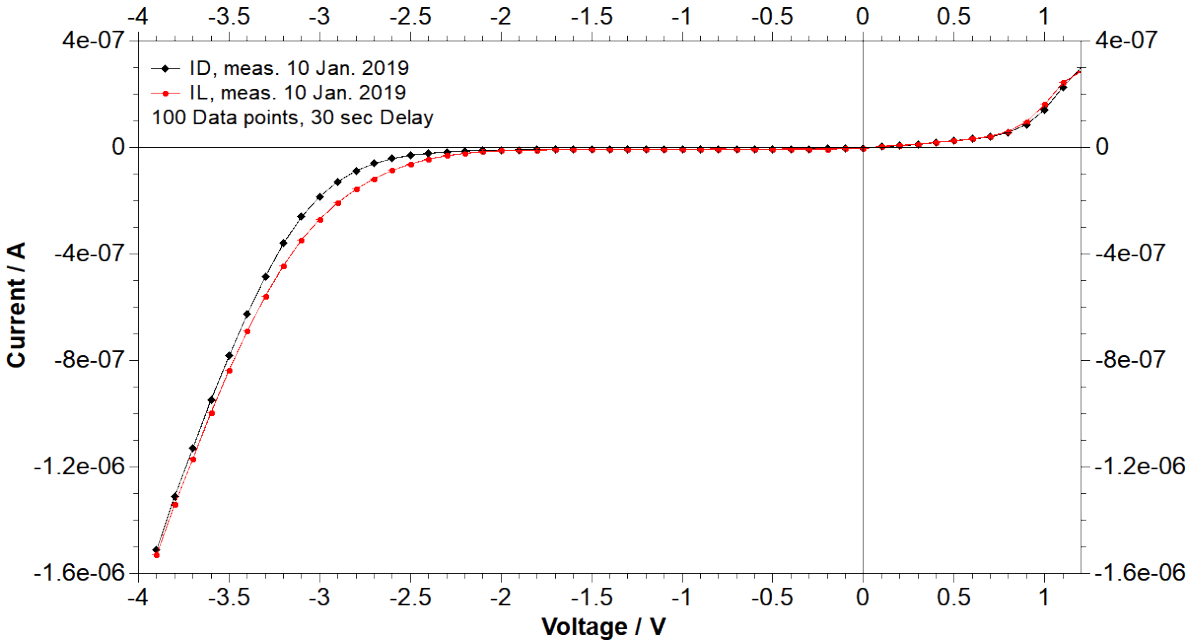

Figure 9.5.: I/V-curve of PEDOT:PSS/P3P4T:PyC$_{60}$ (1:1 w/w)/Al on glass; Fabricated: 26 June 2018
ID... Dark current IL... Current with LED, illuminance: (75 700 ± 300) lx

9.3. PEDOT:PSS/P3P4T:PyC$_{60}$/AZO-electrode

To fabricate an organic photodiode with inkjet printing on a tattoo-paper was the main focus of the thesis. The exact layout of such a device with lamination is shown in Figure 9.6 and Figure 9.7a. First both parts are illustrated and fabricated as mentioned in chapter 8. The combination through lamination of PEDOT:PSS and active film onto AZO-electrode is shown as a schematic and an image (Figure 9.7).

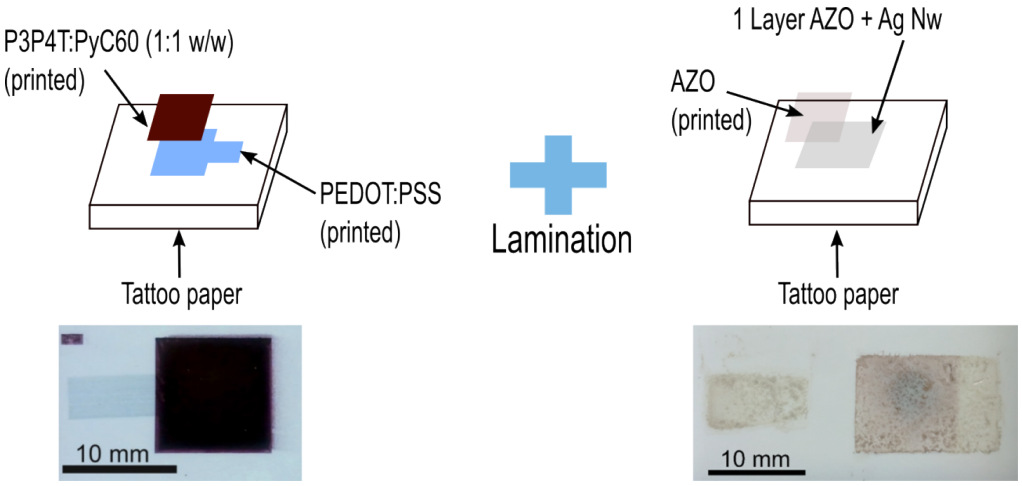

Figure 9.6.: Parts of OPD with P3P4T:PyC$_{60}$ (1:1 w/w) and AZO-electrode

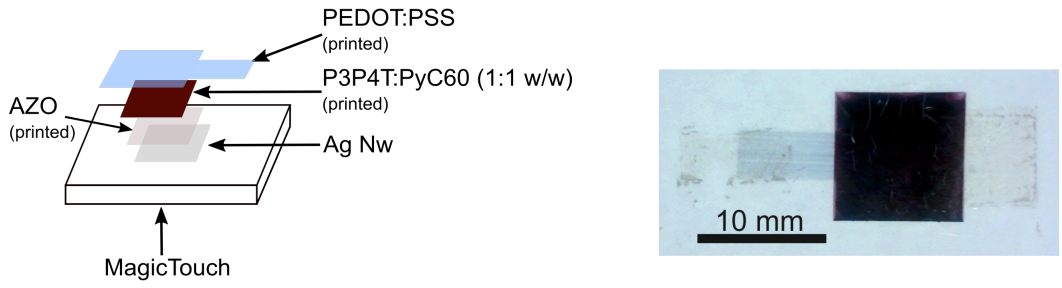

(a) (b)

Figure 9.7.: OPD with P3P4T:PyC$_{60}$ (1:1 w/w) and AZO-electrode as a/an
(a): schematic
(b): image

This layout includes some novelties as it was mostly inkjet printed, has two semi-transparent electrodes and a new material combination of water-soluble polythiophene and fullerene derivatives, all while fabricating onto a transferrable tattoo-paper. Especially the performance and printability of the new blend was doubtful in the beginning.

In section 8.2 the printability of this mixture was shown.

The I/V-curves of a sample with such a layout is given in Figure 9.8. The sample was measured three months after fabrication with (red curve) and without (black curve) illumination from a LED. It shows a diode behaviour with low dark current for reverse bias and a current flow in forward direction. A photo-response is only noticeable in a small range around -1 V, concurrent with a rise of the dark current.

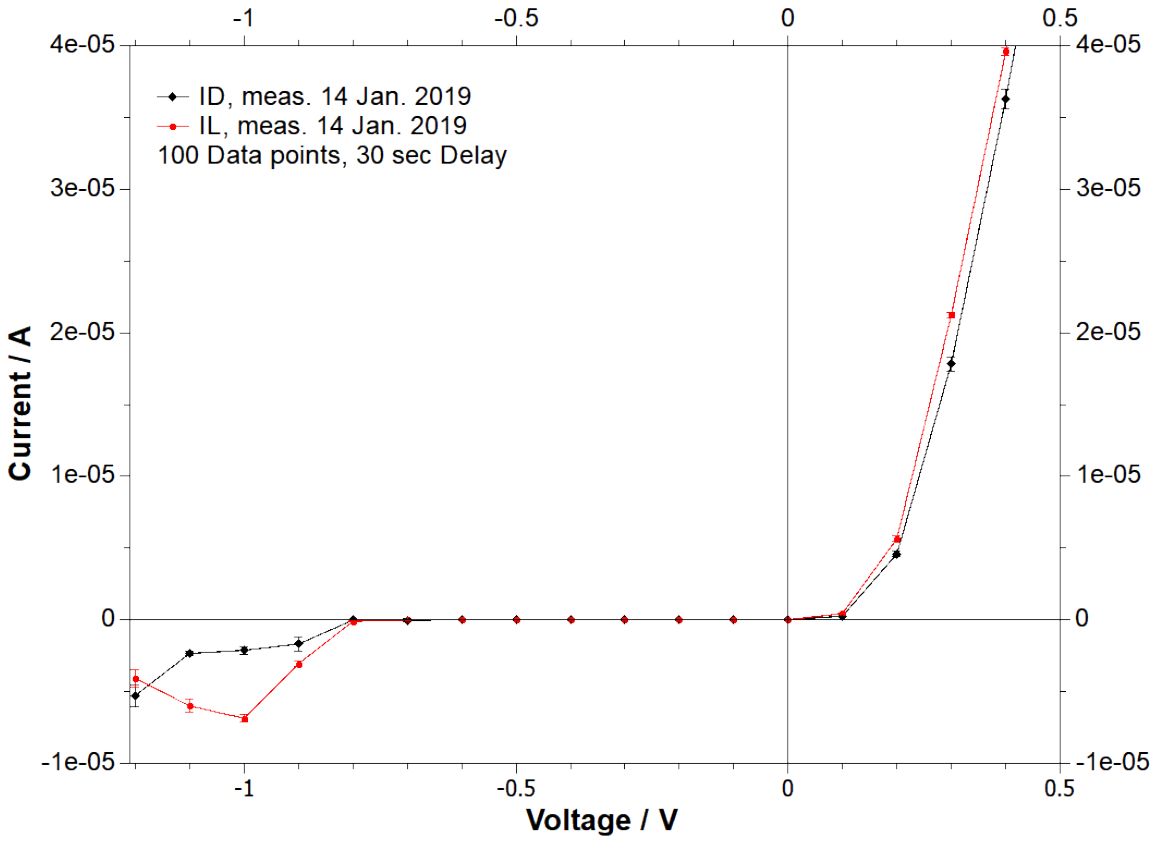

Figure 9.8.: I/V-curve of PEDOT:PSS/P3P4T:PyC$_{60}$ (1:1 w/w)/AZO-electrode on MagicTouch; Fabricated: 10 Oct. 2018
ID... Dark current IL... Current with LED, illuminance: (75 700 ± 300) lx

Part IV.

Summary, conclusion and outlook

10. Summary

The main focus of this thesis was to fabricate an organic bulk heterojunction photodiode onto a conformal, transferrable and commercial substrate. Therefore, different candidates (two decal transfer tattoo-papers and a medical adhesive) were considered and investigated regarding their thickness, roughness, transmittance and their wettability. Based on this characterisation, a decal transfer tattoo-paper called "Tattoo Transfer 2.1" from TheMagicTouch GmbH was chosen, its properties summarised in Table 10.1.

Table 10.1.: Properties of the chosen polymer substrate MagicTouch

R_a(AFM) ... Roughness measured with an AFM on $(10 \times 10)\,\mu$m

θ_M ... Contact angle between substrate and H_2O, averaged between left and right side; for wettability

Transmittance: Range of (350 - 900) nm

Thickness	$\mathbf{R_a}$**(AFM)**	**Transmittance**	$\boldsymbol{\theta_M}$
(608 ± 52) nm	(13 ± 3) nm	$\approx 100\,\%$	$(76 \pm 6)^\circ$

PEDOT:PSS as a semi-transparent electrode was inkjet printed on top of MagicTouch after having carried out a plasma treatment on it, in order to activate its surface. The resulting film showed a thickness of $t \approx 60$ nm, a conductivity $\sigma = (670 \pm 110)$ S/cm and a transmittance of $> 80\,\%$ for (380 - 900) nm.
Different materials and fabrication approaches were chosen for the deposition of the active layer. One with a more common P3HT:ICBA (1:1 w/w) solution and one water-based blend (P3P4T:PyC_{60} (1:1 w/w)), which could be inkjet printed. The inkjet printed P3P4T:PyC_{60} (1:1 w/w) film had a thickness of $t = (260 \pm 30)$ nm, while the spin coated P3HT:ICBA (1:1 w/w) is $t = (230 \pm 40)$ nm thick, measured on comparable samples prepared on glass.
The second electrode was either made through evaporating Al or fabricating a semi-transparent electrode consisting of AZO and Ag Nw. This combination showed only a transmittance of $> 40\,\%$ in the range of (380 - 900) nm.
Details of the fabricated films is found in chapter 8

In the end the best result for an OPD on the tattoo-paper was achieved when using a PEDOT:PSS/P3HT:ICBA (1:1 w/w)/Al layout, where a photodiode behaviour is well observable (section 9.1). The transfer affected the performance negatively. Nevertheless, the device was still functioning afterwards and maintained its functionality over time, despite not storing it in a protected environment.
For the P3P4T:PyC_{60} (1:1 w/w) blend the results either with Al or the AZO-electrode were not satisfying as a photo-response could not be clearly identified. Results related to this blend are reported in section 9.2 and section 9.3.

11. Conclusion and outlook

The first and foremost goal of realising an OPD on a flexible, conformable and transferrable substrate could be accomplished. Samples with a layout of PEDOT:PSS/ P3HT:ICBA (1:1 w/w)/ Al showed the desired I/V-characteristic of a photodiode, despite a more extensive and complete evaluation on several samples was not possible due to time limitations. Obtaining the best performance was not targeted and was therefore neither prioritised nor quantified.

Concerns and effects of time stability as well as the effect of the transfer process could not be fully investigated. First indications verify initial concerns that both time (especially in a non protective environment) and transfer process can negatively affect the OPD performance, with the transfer affecting the forward direction even more (seen in Figure 9.2 and Figure 9.3). Nevertheless, the transfer is not destroying the device fully. In forward bias the curve after transfer of the layout PEDOT:PSS/P3HT:ICBA (1:1 w/w)/ Al did not behave consistently for the investigated samples, although in both cases the threshold (for current flow) shifted to higher voltages and its rise dampened. This was related to a degradation of the OPD, which is also observable in the light-response. As the voltage, where dark and illuminated current differ, is pushed to lower voltages in reverse bias.

Although in the end only inkjet printed OPDs with a weak light-response can be shown, some accomplishments were still achieved. Firstly, an OPD could be fabricated with non-vacuum based processes onto a transferrable, commercial tattoo-paper. Secondly, a novel water-soluble active film consisting of P3P4T and PyC_{60} that is inkjet printable was investigated. Printing parameters for this blend were found and it was possible to incorporate such an active film into the device structure.
For the new water-soluble blend P3P4T:PyC_{60} (1:1 w/w) only poor results were achieved concerning photo-responsitivity. Only in a very narrow region a response could be detected. As the samples were at least two months old when measuring, degradation was expected and will be mainly responsible for reduced functionality. Although the printed layer was satisfactory during first trails, a better investigation into its homogeneity would be beneficial, as sometimes some waviness in the film was observed as a result of the printing process. Nonetheless achieving a decent printed layer with a novel blend of water-soluble polythiophene and fullerene derivatives (P3P4T:PyC_{60} (1:1 w/w)) can be considered a good result and a first step towards a complete understanding and incorporation in a functioning device.

Improving performance of the OPD, either through different additional layers, encapsulation or trying to minimise the degradation during transfer, are all viable options. Laminating an acrylic glue sheet for encapsulation might be an option, as it could even dampen the induced stress in the other layers occurring during transfer.
One could also consider using one of the other water-soluble polythiophenes as their properties vary. As seen in the work of Thalluri *et al.* [78] the hole mobility can vary by two orders of magnitude for different derivatives. Furthermore, the HOMO-level of such derivatives is slightly changing (from -5.02 eV to -5.20 eV) and therefore might impact the energy structure, which was not optimised and might also yield further improvement.

Using a second semi-transparent electrode made of Ag Nw and AZO, even if some concerns about affecting the transfer process remain, was shown to be a manageable approach. Its transmittance was not as high as expected, which was also lowered due to the use of glue during transfer onto glass.
Attempts made so far showed that the transfer is less affected when using brush-painting for the deposition of Ag Nw from a dispersion in isopropyl alcohol. This could be a valid alternative to pursue further as the amount of dispensed Ag Nw seems crucial. Another deposition technique for Ag Nw that could be successful is spray coating. There also a better control over the deposited amount and distribution would be possible.

Bibliography

1. Bandodkar, A. J., Jia, W. & Wang, J. Tattoo-Based Wearable Electrochemical Devices: A Review. *Electroanalysis* **27,** 562–572 (Mar. 2015) (cit. on pp. 3, 6).
2. Liu, Y., Pharr, M. & Salvatore, G. A. Lab-on-Skin: A Review of Flexible and Stretchable Electronics for Wearable Health Monitoring. *ACS Nano* **11,** 9614–9635 (Oct. 2017) (cit. on p. 3).
3. Ferrari, L. M. *et al.* Ultraconformable Temporary Tattoo Electrodes for Electrophysiology. *Advanced Science* **5,** 1700771 (Mar. 2018) (cit. on pp. 3, 5).
4. Al-Halhouli, A., Qitouqa, H., Alashqar, A. & Abu-Khalaf, J. Inkjet Printing for the Fabrication of Flexible/Stretchable Wearable Electronic Devices and Sensors. *Sensor Review* **38,** 438–452 (Mar. 2018) (cit. on pp. 3, 19).
5. Lai, S. *et al.* Ultra-Conformable Organic Field-Effect Transistors and Circuits for Epidermal Electronic Applications. *Organic Electronics* **46,** 60–67 (July 2017) (cit. on pp. 3, 5).
6. Jia, W., Valdés-Ramírez, G., Bandodkar, A. J., Windmiller, J. R. & Wang, J. Epidermal Biofuel Cells: Energy Harvesting from Human Perspiration. *Angewandte Chemie* **125,** 7374–7377 (July 2013) (cit. on p. 3).
7. Kim, J. *et al.* Miniaturized Battery-Free Wireless Systems for Wearable Pulse Oximetry. *Advanced Functional Materials* **27,** n/a–n/a (Jan. 2017) (cit. on pp. 3, 5, 6).
8. Lamprecht, B., Thünauer, R., Ostermann, M., Jakopic, G. & Leising, G. Organic Photodiodes on Newspaper. *physica status solidi (a)* **202,** R50–R52 (Apr. 2005) (cit. on pp. 4, 10).
9. Cantarella, G. *et al.* Buckled Thin-Film Transistors and Circuits on Soft Elastomers for Stretchable Electronics. *ACS Applied Materials & Interfaces* **9,** 28750–28757 (Aug. 2017) (cit. on p. 5).
10. Barsotti, J. *et al.* Ultraconformable Freestanding Capacitors Based on Ultrathin Polyvinyl Formal Films. *Advanced Electronic Materials* **4,** 1800215 (2018) (cit. on p. 5).
11. Reuveny, A. *et al.* High-Frequency, Conformable Organic Amplifiers. *Advanced Materials* **28,** 3298–3304 (2016) (cit. on p. 5).
12. Zimmermann, J. *et al.* Ultrathin Fully Printed Light-Emitting Electrochemical Cells with Arbitrary Designs on Biocompatible Substrates. *Advanced Materials Technologies* **0,** 1800641 (cit. on p. 5).

13. Zucca, A. *et al.* Tattoo Conductive Polymer Nanosheets for Skin-Contact Applications. *Advanced Healthcare Materials* **4,** 983–990 (May 2015) (cit. on p. 5).

14. Yokota, T. *et al.* Ultraflexible Organic Photonic Skin. *Science Advances* **2,** e1501856 (Apr. 2016) (cit. on p. 5).

15. Bandodkar, A. J. *et al.* Tattoo-Based Potentiometric Ion-Selective Sensors for Epidermal pH Monitoring. *Analyst* **138,** 123–128 (Nov. 2012) (cit. on p. 6).

16. Bandodkar, A. J. *et al.* Epidermal Tattoo Potentiometric Sodium Sensors with Wireless Signal Transduction for Continuous Non-Invasive Sweat Monitoring. *Biosensors and Bioelectronics* **54,** 603–609 (Apr. 2014) (cit. on p. 6).

17. Jia, W., Valdés-Ramírez, G., Bandodkar, A. J., Windmiller, J. R. & Wang, J. Epidermal Biofuel Cells: Energy Harvesting from Human Perspiration. *Angewandte Chemie International Edition* **52,** 7233–7236 (2013) (cit. on p. 6).

18. Hu, S., Shi, Z., Zhao, W., Wang, L. & Yang, G. Multifunctional Piezoelectric Elastomer Composites for Smart Biomedical or Wearable Electronics. *Composites Part B: Engineering* **160,** 595–604 (Mar. 2019) (cit. on p. 6).

19. Park, J. H., Wu, C., Sung, S. & Kim, T. W. Ingenious Use of Natural Triboelectrification on the Human Body for Versatile Applications in Walking Energy Harvesting and Body Action Monitoring. *Nano Energy* **57,** 872–878 (Mar. 2019) (cit. on p. 6).

20. Yang, Z., Deng, J., Sun, X., Li, H. & Peng, H. Stretchable, Wearable Dye-Sensitized Solar Cells. *Advanced Materials* **26,** 2643–2647 (May 2014) (cit. on p. 6).

21. Kaltenbrunner, M. *et al.* Ultrathin and Lightweight Organic Solar Cells with High Flexibility. *Nature Communications* **3,** 770 (Apr. 2012) (cit. on p. 6).

22. Kaltenbrunner, M. *et al.* Flexible High Power-per-Weight Perovskite Solar Cells with Chromium Oxide–Metal Contacts for Improved Stability in Air. *Nature Materials* **14,** 1032–1039 (Oct. 2015) (cit. on p. 6).

23. Yoon, J. *et al.* 65.1: Invited Paper: World 1st Large Size 18-Inch Flexible OLED Display and the Key Technologies. *SID Symposium Digest of Technical Papers* **46,** 962–965 (2015) (cit. on p. 7).

24. Stavrinidou, E. *et al.* Electronic Plants. *Science Advances* **1,** e1501136 (Nov. 2015) (cit. on p. 7).

25. Irimia-Vladu, M. "Green" Electronics: Biodegradable and Biocompatible Materials and Devices for Sustainable Future. *Chemical Society Reviews* **43,** 588–610 (Dec. 2013) (cit. on p. 7).

26. Bao, Q., Braun, S., Wang, C., Liu, X. & Fahlman, M. Interfaces of (Ultra)Thin Polymer Films in Organic Electronics. *Advanced Materials Interfaces* **6,** 1800897 (2019) (cit. on p. 7).

27. Shinar, R. & Shinar, J. *Organic Electronics in Sensors and Biotechnology* OCLC: 464640045. ISBN: 978-0-07-159676-3 978-0-07-173803-3 978-0-07-159675-6 978-7-159-60075-6. http://accessengineeringlibrary.com/browse/organic-electronics-in-sensors-and-biotechnology (2019) (McGraw-Hill, New York, 2009) (cit. on p. 7).

28. Bloor, D. & Blythe, T. *Electrical Properties of Polymers* OCLC: 470979726. ISBN: 978-0-521-55838-9 (Cambridge University Press, Cambridge, 2008) (cit. on p. 7).

29. Baeg, K.-J., Binda, M., Natali, D., Caironi, M. & Noh, Y.-Y. Organic Light Detectors: Photodiodes and Phototransistors. *Advanced Materials* **25,** 4267–4295 (Aug. 2013) (cit. on pp. 7–9, 11, 12).

30. Rafique, S., Abdullah, S. M., Sulaiman, K. & Iwamoto, M. Fundamentals of Bulk Heterojunction Organic Solar Cells: An Overview of Stability/Degradation Issues and Strategies for Improvement. *Renewable and Sustainable Energy Reviews* **84,** 43–53 (Mar. 2018) (cit. on pp. 9, 12).

31. Dogru, M. & Bein, T. On the Road towards Electroactive Covalent Organic Frameworks. *Chem. Commun.* **50,** 5531–5546 (2014) (cit. on p. 9).

32. Ostroverkhova, O. Organic Optoelectronic Materials: Mechanisms and Applications. *Chemical Reviews* **116,** 13279–13412 (Nov. 2016) (cit. on pp. 10, 12).

33. Gong, X. *et al.* High-Detectivity Polymer Photodetectors with Spectral Response from 300 Nm to 1450 Nm. *Science* **325,** 1665–1667. pmid: 19679770 (Sept. 2009) (cit. on p. 11).

34. Shi, L. *et al.* Research Progress in Organic Photomultiplication Photodetectors. *Nanomaterials* **8,** 713 (Sept. 2018) (cit. on p. 12).

35. Jansen-van Vuuren, R. D., Armin, A., Pandey, A. K., Burn, P. L. & Meredith, P. Organic Photodiodes: The Future of Full Color Detection and Image Sensing. *Advanced Materials* **28,** 4766–4802 (June 2016) (cit. on p. 12).

36. Manna, E., Xiao, T., Shinar, J. & Shinar, R. Organic Photodetectors in Analytical Applications. *Electronics* **4,** 688–722 (Sept. 2015) (cit. on p. 12).

37. Elkington, D., Cooling, N., Zhou, X. J., Belcher, W. J. & Dastoor, P. C. Single-Step Annealing and Encapsulation for Organic Photovoltaics Using an Exothermically-Setting Encapsulant Material. *Solar Energy Materials and Solar Cells* **124,** 75–78 (May 2014) (cit. on p. 12).

38. Peters, C. H. *et al.* High Efficiency Polymer Solar Cells with Long Operating Lifetimes. *Advanced Energy Materials* **1,** 491–494 (2011) (cit. on p. 12).

39. Romero-Gomez, P. *et al.* Enhanced Stability in Semi-Transparent PTB7/PC71BM Photovoltaic Cells. *Solar Energy Materials and Solar Cells* **137,** 44–49 (June 2015) (cit. on p. 12).

40. Deckman, I., Lechêne, P. B., Pierre, A. & Arias, A. C. All-Printed Full-Color Pixel Organic Photodiode Array with a Single Active Layer. *Organic Electronics* **56,** 139–145 (May 2018) (cit. on p. 12).

41. Khan, Y. *et al.* A Flexible Organic Reflectance Oximeter Array. *Proceedings of the National Academy of Sciences* **115,** E11015–E11024. pmid: 30404911 (Nov. 2018) (cit. on p. 12).

42. Ryu, G. *et al.* Flexible and Printed PPG Sensors for Estimation of Drowsiness. *IEEE Transactions on Electron Devices* **65,** 2997–3004 (July 2018) (cit. on p. 13).

43. Lim, C.-J., Kim, J.-H. & Park, J.-W. Highly Flexible and Solution-Processed Organic Photodiodes and Their Application to Optical Luminescent Oxygen Sensors. *Organic Electronics* **65,** 100–109 (Feb. 2019) (cit. on p. 13).

44. Nam, G.-H., Kim, K. & Chung, D. S. Non-Power-Driven Organic Photodiode via Junction Engineering. *Nanotechnology* **30,** 055202 (Dec. 2018) (cit. on p. 13).

45. Strobel, N., Eckstein, R., Lehr, J., Lemmer, U. & Hernandez-Sosa, G. Semiconductor:Insulator Blends for Speed Enhancement in Organic Photodiodes. *Advanced Electronic Materials* **4,** 1700345 (2018) (cit. on p. 13).

46. Takata, Y., Hidaka, S. & Kohno, M. Wettability Improvement by Plasma Irradiation and Its Applications to Phase-Change Phenomena. *Heat Transfer Engineering* **30,** 549–555 (June 2009) (cit. on p. 16).

47. Ebnesajjad, S. in *Surface Treatment of Materials for Adhesive Bonding* 227–269 (Elsevier, 2014). ISBN: 978-0-323-26435-8. https://linkinghub.elsevier.com/retrieve/pii/B9780323264358000095 (2019) (cit. on p. 16).

48. Cullen, P. J. *et al.* Translation of Plasma Technology from the Lab to the Food Industry. *Plasma Processes and Polymers* **15,** 1700085 (Feb. 2018) (cit. on p. 16).

49. Wiemer, M., Wuensch, D., Braeuer, J. & Gessner, T. in *Handbook of Wafer Bonding* (eds Ramm, P., Lu, J. J.-Q. & Taklo, M. M. V.) 101–118 (Wiley-VCH Verlag GmbH & Co. KGaA, Weinheim, Germany, Feb. 2012). ISBN: 978-3-527-64422-3 978-3-527-32646-4. http://doi.wiley.com/10.1002/9783527644223.ch6 (2019) (cit. on p. 16).

50. Emslie, A. G., Bonner, F. T. & Peck, L. G. Flow of a Viscous Liquid on a Rotating Disk. *Journal of Applied Physics* **29,** 858–862 (May 1958) (cit. on p. 16).

51. Sahu, N., Parija, B. & Panigrahi, S. Fundamental Understanding and Modeling of Spin Coating Process: A Review. *Indian Journal of Physics* **83,** 493–502 (Apr. 2009) (cit. on pp. 16, 17).

52. Cummins, G. & Desmulliez, M. P. Inkjet Printing of Conductive Materials: A Review. *Circuit World* **38,** 193–213 (Nov. 2012) (cit. on pp. 17–19).

53. Prudenziati, M. & Hormadaly, J. in *Printed Films* (eds Prudenziati, M. & Hormadaly, J.) 3–29 (Woodhead Publishing, Jan. 2012). ISBN: 978-1-84569-988-8. http://www.sciencedirect.com/science/article/pii/B9781845699888500011 (2018) (cit. on pp. 18, 19).

54. Singh, M., Haverinen, H. M., Dhagat, P. & Jabbour, G. E. Inkjet Printing—Process and Its Applications. *Advanced Materials* **22,** 673–685 (Feb. 2010) (cit. on p. 18).

55. Shah, S. I., Jaffari, G. H., Yassitepe, E. & Ali, B. Chapter 4 - Evaporation : Processes, Bulk Microstructures, and Mechanical Properties, 118 (cit. on p. 19).

56. Schmit, J., Creath, K. & Wyant, J. C. in *Optical Shop Testing* (ed Malacara, D.) 667–755 (John Wiley & Sons, Inc., Hoboken, NJ, USA, June 2007). ISBN: 978-0-470-13597-6 978-0-471-48404-2. http://doi.wiley.com/10.1002/9780470135976.ch15 (2019) (cit. on p. 19).

57. Johnson, D., Hilal, N. & Bowen, W. R. in *Atomic Force Microscopy in Process Engineering* 1–30 (Elsevier, 2009). ISBN: 978-1-85617-517-3. http://linkinghub.elsevier.com/retrieve/pii/B9781856175173000018 (2018) (cit. on p. 20).

58. Hofmann, A. in *Principles and Techniques of Biochemistry and Molecular Biology* (eds Wilson, K. & Walker, J.) 7th ed., 477–521 (Cambridge University Press, Cambridge, 2010). ISBN: 978-0-511-84147-7. https://www.cambridge.org/core/product/identifier/CBO9780511841477A119/type/book_part (2018) (cit. on pp. 20, 21).

59. Letellier, P., Mayaffre, A. & Turmine, M. Drop Size Effect on Contact Angle Explained by Nonextensive Thermodynamics. Young's Equation Revisited. *Journal of Colloid and Interface Science* **314,** 604–614 (Oct. 2007) (cit. on p. 21).

60. Smits, F. M. Measurement of Sheet Resistivities with the Four-Point Probe. *The Bell System Technical Journal* **37,** 711–718 (May 1958) (cit. on p. 22).

61. Schroder, D. *Semiconductor Material and Device Characterization* ISBN: 978-0-471-73906-7 (IEEE Press; Wiley, Piscataway NJ; Hoboken N.J., 2006) (cit. on p. 22).

62. Valdes, L. B. Resistivity Measurements on Germanium for Transistors. *Proceedings of the IRE* **42,** 420–427 (Feb. 1954) (cit. on p. 22).

63. *Poly(3-Hexylthiophene-2,5-Diyl), Regioregular Electronic Grade* http://riekemetals.com/products-services/compound/2041 (2019) (cit. on p. 26).

64. *Poly[3-(Potassium-4-Butanoate)Thiophene-2,5-Diyl], Regioregular* http://www.riekemetals.com/products-services/compound/2060 (2018) (cit. on p. 26).

65. *Poly[3-(Potassium-5-Pentanoate)Thiophene-2,5-Diyl], Regioregular* http://www.riekemetals.com/products-services/compound/2061- (2018) (cit. on p. 26).

66. *Poly[3-(Potassium-6-Hexanoate)Thiophene-2,5-Diyl], Regioregular* http://www.riekemetals.com/products-services/compound/2063- (2018) (cit. on p. 26).

67. *Poly[3-(Potassium-7-Heptanoate)Thiophene-2,5-Diyl], Regioregular* http://www.riekemetals.com/products-services/compound/2065- (2018) (cit. on p. 26).

68. *C_{60} Pyrrolidine Tris-Acid Ethyl Ester 709093* https://www.sigmaaldrich.com/catalog/product/aldrich/709093 (2018) (cit. on p. 26).

69. *ICBA 753955* https://www.sigmaaldrich.com/catalog/product/aldrich/753955 (2019) (cit. on p. 26).

70. *Clevious P Jet 700* https://www.heraeus.com/media/media/hec/documents_hec/data_sheets_hep/Clevios_P_JET_700.pdf (2019) (cit. on pp. 28, 56).

71. Shi, H., Liu, C., Jiang, Q. & Xu, J. Effective Approaches to Improve the Electrical Conductivity of PEDOT:PSS: A Review. *Advanced Electronic Materials* **1,** 1500017 (2015) (cit. on p. 56).

72. Dallinger, A. *Ultrathin, Adhesive Skin-Contact Electrodes* Master Thesis (Graz University of Technology, 2019) (cit. on pp. 56, 57).

73. Lövenich, W. PEDOT-Properties and Applications. *Polymer Science Series C* **56,** 135–143 (Sept. 2014) (cit. on p. 56).

74. Huang, J., Miller, P., de Mello, J., de Mello, A. & Bradley, D. Influence of Thermal Treatment on the Conductivity and Morphology of PEDOT/PSS Films. *Synthetic Metals* **139,** 569–572 (Oct. 2003) (cit. on p. 60).

75. Friedel, B. *et al.* Effects of Layer Thickness and Annealing of PEDOT:PSS Layers in Organic Photodetectors. *Macromolecules* **42,** 6741–6747 (Sept. 2009) (cit. on p. 60).

76. Walker, S. B. & Lewis, J. A. Reactive Silver Inks for Patterning High-Conductivity Features at Mild Temperatures. *Journal of the American Chemical Society* **134,** 1419–1421 (Jan. 2012) (cit. on p. 62).

77. *Aluminum-Doped Zinc Oxide Ink for Inkjet Printing — Sigma-Aldrich* https://www.sigmaaldrich.com/catalog/product/aldrich/901065?lang=de&region=AT (2019) (cit. on p. 62).

78. Thalluri, G. K. V. V. *et al.* Opto-Electrical and Morphological Characterization of Water Soluble Conjugated Polymers for Eco-Friendly Hybrid Solar Cells. *Solar Energy Materials and Solar Cells* **95,** 3262–3268 (Dec. 2011) (cit. on p. 80).